February 6, 2019

Disclaimer:

This report is unfinished and still a work in progress. It has written been written based on analysis of the 60H dataset with the tag 5033A. Any results and text past Chapter 2 (the analysis procedures) are subject to change, especially once the new dataset is available. Chapter 2 itself will probably be improved going forward. Don't take results or methods as final.

- Nick Kinnaird

Analysis Note for 60H Dataset Relative Unblinding

Nick Kinnaird - Boston University

February 6, 2019

High Level Summary

- Lead Analysts: Nick Kinnaird, James Mott
- Positron Reconstruction Method: Recon West
- Software Release: v9_11_00
- Dataset: gm2pro_daq_full_run1_60h_5033A_withfullDQC (waiting for final production)
- Histogramming Method: Ratio
- Gain Correction Method: Default in reconstruction
- Pileup Correction Method: Asymmetic shadow window, doublets only
- Lost Muon Spectrum Extraction: Triple coincidence, not included in ratio fit
- Model for CBO: Exponential envelope, frequency from tracking analysis
- Model for VW: Exponential envelope, constant frequency, not included in ratio fit
- Fit Range: $30\,\mu\text{s} - 500\,\mu\text{s}$
- $R = -19.88 \pm 1.373\,\text{ppm} \pm XX\text{ppm}$ (blinding with common string)
- $\chi^2/NDF = 3052/3145$
- P value = 0.8806

Final fit function:

$$R(t) = \frac{2f(t) - f_+(t) - f_-(t)}{2f(t) + f_+(t) + f_-(t)}$$

$$f_\pm(t) = f(t \pm T_a/2)$$

$$f(t) = N_{cbo}(t) \cdot (1 + A\cos(\omega_a t + \phi))$$

$$N_{cbo}(t) = 1 + A_{cbo-N} \cdot e^{-t/\tau_{cbo}} \cdot \cos(\omega_{cbo}(t) \cdot t + \phi_{cbo-N})$$

$$\omega_a = 2\pi \cdot 0.2291\,\text{MHz} \cdot (1 + R \times 10^{-6})$$

Chapter 1

Introduction

This report details the analysis procedures, results, and systematic studies I carried out for the "60H" dataset acquired during Run 1 in 2018 of the Fermilab Muon $g-2$ Experiment, E989. The 60H dataset was gathered from April 22nd to 24th, 2018, with runs 15921 - 15992. The quad voltages used were 13.1 and 18.3 kV, corresponding to an approximate n value of 0.10843 (DocDB 11547). The kicker voltage range was 128 - 132 kV. Nearly 10^9 positrons were collected during this period, corresponding to about 10% of the BNL statistics gathered (DocDB 15217).

In Chapter 2 I detail the analysis procedures used. This includes information on how the data are prepared, starting after the "production" stage and leading up to the construction of histograms. The application of gain corrections, pileup construction, the extraction of lost muons, and other various data preparation procedures are described briefly. Also included are various models used in the fitting of the data, including coherent betatron oscillation (CBO) effects and the lost muon function.

In Chapter 3 I detail the results of the analysis. This includes the application of the pileup correction, the fits to the data and subsequent residuals and FFTs of those residuals, and start time scans. Results are shown for all calorimeters added together and for individual calorimeters.

In Chapter 4 I detail the results of systematic studies to the data and fits, which is the real meat of the analysis. This includes studies relating to corrections applied (gain, pileup, etc.), as well as models used within the fit (CBO, lost muons, VW, etc.). Also included are various studies related to items like the bin width or randomization used in the analysis.

Chapter 5 summarizes the final results of the report, as well as next steps for the analysis. There is also an Appendix A which provides some derivations for the ratio method used in fitting the data.

Chapter 2

Analysis Procedures

2.1 Key parameters in reconstruction method

Default parameters used in the Recon West production of the 60H dataset, with SAM dataset name "gm2pro_daq_full_run1_60h_5033A_withfullDQC".

2.2 Analysis Data Preparation Procedure

- git branch: gm2analyses branch feature/KinnairdAnalyses
- Majority of code located under gm2analyses/macros/RatioMacro

1. Submit jobs to OSG to run the rootTreesAndLostMuons.fcl file which produces `ROOT` trees of positron hits using the ClusterTree analyzer module and coincident MIP hits using the TestCoincidenceFinder analyzer module.

2. Submit jobs to Fermigrid to produce histograms from `ROOT` trees using the ClusterTreeToHistsPileup.C macro in RatioMacro/HistMaking, 1 job per `ROOT` tree. Beyond standard e^+ arrival time histograms this macro produces pileup and lost muon histograms all within the same `ROOT` file.

3. ClusterTreeToHistsPileup.C uses a single random seed for all randomization during histogram making. The default for the random seed is the hash of the input `ROOT` file name so that results can be reproduced on the grid, and so that each individual grid job uses a unique random seed.

2.3 Histogramming Procedure

Method: Ratio (DocDB 13080)
Systematics Sections 4.6.1 and 4.6.2

1. Loop through all clusters and apply an artificial deadtime (ADT) to combine hits within 6 ns into a single pulse using the same procedure and code that the pileup method uses (see below). Drop clusters with time $< 25\,\mu$s or time $> 660\,\mu$s.

2. Histograms are constructed with `ROOT`'s `TH1F` class with 149.15 ns bins from $0 - 699.960\,95\,\mu$s corresponding to 4693 bins, of which 4258 are filled with data, and 3151 are fit with a fit range of $30\,\mu\text{s} - 500\,\mu$s.

3. Randomize cluster times by $\pm 149.15/2$ ns and fill histograms for energies > 1.7 GeV. Randomization uses `ROOT`'s default `TRandom3` class.

4. Divide the data into four datasets by filling one of the four histograms $\{u_+(t), u_-(t), v_1(t), v_2(t)\}$ per cluster. The associated histogram is determined by generating a random number between 0 and 1, and comparing that number to the relative probabilities of the different weights:

$$u_+(t) : u_-(t) : v_1(t) : v_2(t) = e^{T/2\tau} : e^{-T/2\tau} : 1 : 1 \tag{2.1}$$

   τ is the lifetime of the muon, taken at $64.4\,\mu$s. See the appendix for more details on what this weighting scheme does.

5. Clusters filled into the $u_+(t)$ histogram have their times shifted by $t \to t - T_a/2$ and clusters filled into the $u_-(t)$ histogram have their times shifted by $t \to t + T_a/2$.

6. T_a is known a priori to high precision from the previous experiment, and its value is taken as $1/f_a$, where f_a is 0.229 073 5 MHz:

$$T_a \approx 4.365\,411\,\mu\text{s} \tag{2.2}$$

   This value for f_a was determined by averaging column 2 of Table XV of the E821 Final Report, which consits of the f_a results for the different run periods in that experiment. A systematic error on the choice of this parameter is calculated in Section 4.6.1.

2.4 Gain Correction Procedure

Gain correction method: Default by the Italian Calibration Team (DocDB 16003)
Systematics Section 4.1

1. Long term gain is corrected using out-of-fill laser shots including normalization from the Source Monitor.

2. In-fill gain is corrected using in-fill laser shots including normalization from the Source Monitor.

3. Short-term double pulse (SDTP) effect is not yet included, but will be for the final report.

2.5 Pileup Correction Procedure

Pileup correction method: Asymmetric shadow window (DocDB 14394 and DocDB 14830)
Systematics Section 4.2

1. Create a vector of clusters per calorimeter per fill. For each cluster look for a second cluster in a window from 12-18 ns after the time of the first cluster. This corresponds to a shadow dead time (SDT) of 6 ns and a shadow gap time (SGT) of 12 ns, equal to 1 and 2 times the applied ADT respectively.

2. Create shadow doublets with energies and times as:

$$E_{doublet} = C \cdot (E_1 + E_2), \tag{2.3}$$

$$t_{doublet} = \frac{t_1 \cdot E_1 + (t_2 - SGT) \cdot E_2}{E_1 + E_2}, \tag{2.4}$$

   where the latter equation is the energy-weighted average of the times of the two singlets. In the former equation, the calculation of the doublet energy is the sum of the singlets times some calibration factor. That factor is set equal to 1, which is a reasonable approximation since the spatial separation in the reconstruction is turned off. The systematic effects of a factor not equal to 1 are studied in Section 4.2.2.

3. Randomize $t_{doublet}$ times by $\pm 149.15/2$ ns as in the histogramming procedure described above.

4. For each calorimeter construct a pileup spectrum P = doublets - singlets = D - S, where the singlets are subtracted at time $t_{doublet}$ as opposed to their individual times, and pulses are only added or subtracted if they are above 1.7 GeV. Subtract P off energy and threshold histograms.

5. For pileup subraction in the ratio method, randomly split doublets and singlets into 4 separate histograms as is done in the histogramming procedure described above, with times shifted accordingly. Doublets and their associated singlets are put in the same histogram. Subtract 4 pileup histograms from corresponding $\{u_+(t), u_-(t), v_1(t), v_2(t)\}$ histograms before forming the ratio.

6. The errors of the pileup corrected histogram were determined to be:

$$\sigma(N_{corrected}) = \sqrt{N_{corrected} + 2N_1 + 6N_4}, \tag{2.5}$$

   where N_1 is the number of doublets where both singlets were below threshold, and N_4 is the number of doublets where both singlets were above threshold, and this is a quantity evaluated at each time bin (DocDB 14830). A histogram of error multipliers was created by factoring out the $N_{corrected}$ term, which is then applied to the bin errors before fitting. This is true even for the ratio errors to good approximation (DocDB 2896 Appendix - John Paley's thesis). Note that I did not time randomize the N_1 and N_4 entries when constructing the correct errors, which is a negligble effect. This is

justified in DocDB 14394 slide 11, which shows that this is about a 2 ppb effect. (The pileup is about a 1% effect, including the pileup errors is about 1% effect on that, and then time randomizing the errors is less than that.)

7. The pileup correction at the triplet/contamination level is not included. It has been determined not be necessary for the 60H and Run 1 data.

2.6 Lost muon spectrum extraction procedure

Method: Triple coincidence of clusters (DocDB 12912)
Systematics Section 4.3

Note that the lost muons are not included in the ratio fit because the ratio method divides out such slow effects. This is reflected by the lack of a low frequency peak in the FFT of the fit residuals for the ratio fit, whereas such a peak exists for T method fits. I include here however my method for extracting the lost muon function for systematic studies.

1. Triple coincidence of clusters in 3 consecutive calorimeters are made with an energy cut of 100 MeV < E < 250 MeV and 5 ns < dt < 8.5 ns.

2. A time histogram is made with the muon cluster in the first calorimeter.

3. The function that would be used in the final fit is:

$$\Lambda(t) = 1 - \kappa_{loss} \int_0^t L(t') e^{(-t'/\gamma\tau_\mu)} dt' \tag{2.6}$$

where $L(t)$ is the histogram of triple concidences, and an arbitrary 10^{-6} factor has been absorbed into κ_{loss} in order to bring it to a more reasonable value (from $\mathcal{O}(10^{-10})$ to $\mathcal{O}(10^{-4})$).

2.7 Beam Dynamics: CBO Model

Systematics Section 4.4

1. The CBO frequency as a function of time is taken from the tracking analysis, DocDB 14208, and shown in Figure 2.1. The CBO frequency is not constant during the measurement time because the quad voltage was not constant as a function of time. As described in that document, the source of this is almost certainly the fact that some

of the quad resistors were damaged, leading to longer RC time constants. The form used is

$$\omega_{cbo}(t) = \omega_0(1 + \Delta\omega t + Ae^{-t/\tau_A} + Be^{-t/\tau_B}), \tag{2.7}$$

with parameters determined from station 12 in the 60H dataset and fixed in the fit as:

$$\begin{aligned} \Delta\omega &= 1.86 \times 10^{-8}\,\mathrm{ns}^{-1}, \\ A &= -0.0504, \\ \tau_A &= 73.3\,\mu\mathrm{s}, \\ B &= -0.131, \\ \tau_B &= 16.6\,\mu\mathrm{s}. \end{aligned}$$

The parameter ω_0 is allowed to float in the fit and starts with a value of $2.3051\,\mathrm{rad}\,\mu\mathrm{s}^{-1}$ The starting guess for the CBO phase is 0. Because the ratio method divides out the CBO partially (reduction by a factor of ~ 5 in the FFT cbo peak amplitude), the ratio method has trouble with letting the other frequency parameters float, and fixing them to slightly different values does not change the fit results significantly. Parameter values determined from station 18 are similar to those from station 12 and were also tested with no significant change in the fit results. See section 4.4.1.

2. Again because the ratio method divides out the CBO partially, the ratio fit has a hard time fitting the CBO lifetime. Therefore τ_{cbo} is fixed to $180\,\mu\mathrm{s}$, determined from a T Method fit to the same data.

3. An exponential function is assumed for the CBO decoherence. Other models are tested in Section 4.4.2.

4. In the added calorimeter fit, the N_{cbo} term is included in the fit, while the N_{2cbo}, A_{cbo}, and ϕ_{cbo} terms are excluded. For the individual calorimeter fits, the latter are all included.

5. The CBO function pieces are:

$$\begin{aligned} N_{cbo}(t) &= 1 + A_{cbo-N} \cdot e^{-t/\tau_{cbo}} \cdot \cos(\omega_{cbo}(t) \cdot t + \phi_{cbo-N}), \\ N_{2cbo}(t) &= 1 + A_{2cbo-N} \cdot e^{-t/\tau_{cbo}} \cdot \cos(2 \cdot \omega_{cbo}(t) \cdot t + \phi_{2cbo-N}), \\ A_{cbo}(t) &= 1 + A_{cbo-A} \cdot e^{-t/\tau_{cbo}} \cdot \cos(\omega_{cbo}(t) \cdot t + \phi_{cbo-A}), \\ \phi_{cbo}(t) &= 1 + A_{cbo-\phi} \cdot e^{-t/\tau_{cbo}} \cdot \cos(\omega_{cbo}(t) \cdot t + \phi_{cbo-\phi}) \end{aligned} \tag{2.8}$$

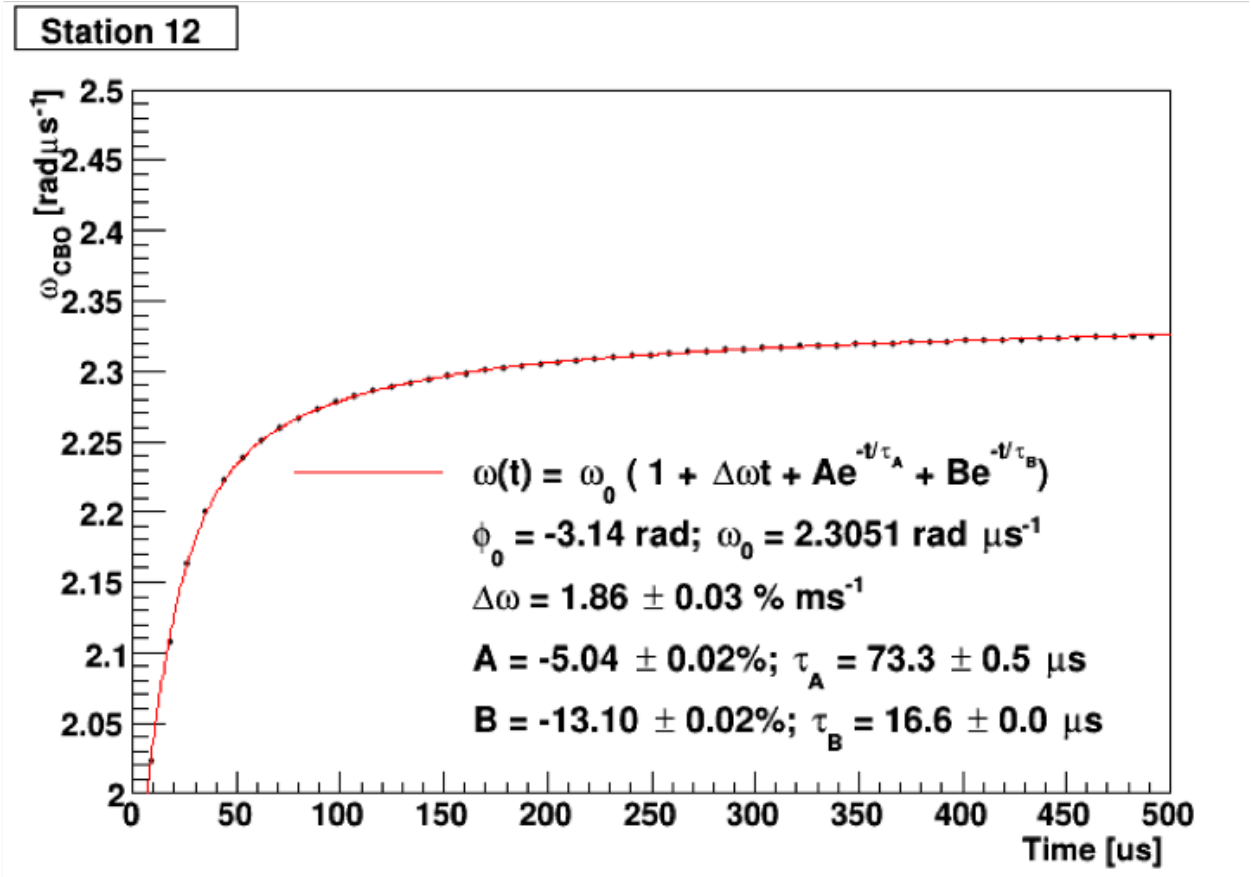

Figure 2.1: CBO frequency determined with tracker data as a function of time, for station 12 in the 60H dataset. The frequency was modeled as a sum of a constant with a linear part and two exponentials. It rises sharply at early times and slowly over the rest of the fill. Plot created by James Mott, DocDB 14208.

2.8 Beam Dynamics: Vertical Waist Model

Systematics Section 4.5

ω_a is senstive to the vertical width of the beam, which is characterized by the frequency

$$f_{VW} = f_{cyc} - 2f_y, \tag{2.9}$$

$$f_y = f_{cbo}\sqrt{\frac{2f_{cyc}}{f_{cbo}} - 1}, \tag{2.10}$$

where f_{cyc} is the cyclotron frequency and f_{cbo} is the radial CBO frequency of the beam. In the 60H dataset $f_{VW} \approx 2.3\,\text{MHz} \approx 10 \cdot \omega_a$, which is an even multiple of the $g-2$ frequency. Any frequencies which are even multiples of the $g-2$ frequency largely cancel in the ratio. This is shown for the vertical waist in Figure 2.2. This combined with the time randomization to remove the fast rotation (f_{cyc}) means the vertical waist does not need to be included in the ratio fit. For systematic studies including the VW the follow are taken:

1. An exponential function is assumed for the VW decoherence as in the CBO, and so the VW term is defined as

$$V(t) = 1 + A_{VW}e^{-t/\tau_{VW}}\cos(\omega_{VW}t + \phi_{VW}) \tag{2.11}$$

2. ω_{VW} is assumed to be a constant value even though the CBO frequency changes vs time.

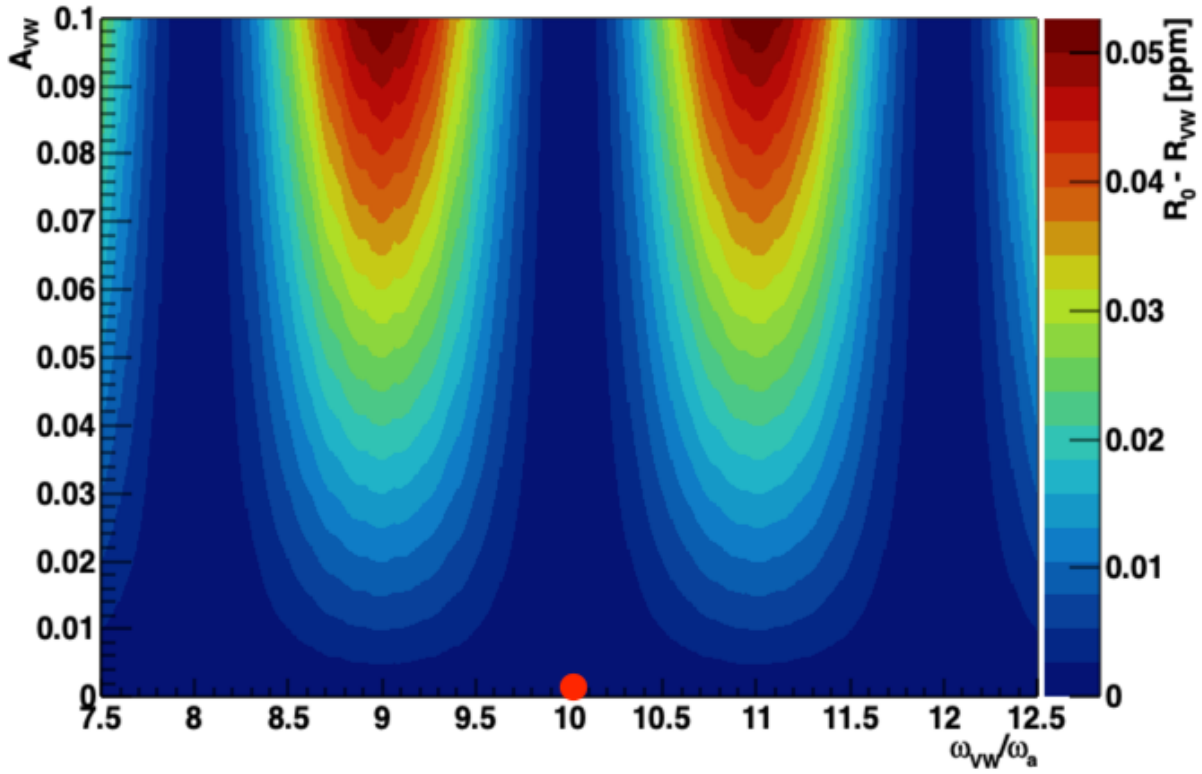

Figure 2.2: Plotted is the difference in the maximum value of the ratio with and without a vertical waist function included, as a function of both the amplitude of the vertical waist effect and the vertical waist frequency in units of the $g-2$ frequency. (Note that this is not R the frequency fit parameter, but the actual value of the ratio fit function.) This plot was created using a `TF1` in `ROOT`. As is shown the difference reaches a minimum for even multiples of the $g-2$ frequency. The 60H dataset lives at the bottom center of this plot, marked by a red circle, where the difference in the ratio is approximately 5×10^{-6} at 30 μs.

2.9 Final Fit Function

The following function is used for the final fit for the calorimeter sum:

$$R(t) = \frac{2f(t) - f_+(t) - f_-(t)}{2f(t) + f_+(t) + f_-(t)} \tag{2.12}$$

$$f_\pm(t) = f(t \pm T_a/2) \tag{2.13}$$

$$f(t) = N_{cbo}(t) \cdot (1 + A\cos(\omega_a t + \phi)) \tag{2.14}$$

$$N_{cbo}(t) = 1 + A_{cbo-N} \cdot e^{-t/\tau_{cbo}} \cdot \cos(\omega_{cbo}(t) \cdot t + \phi_{cbo-N}) \tag{2.15}$$

$$\omega_a = 2\pi \cdot 0.2291\,\text{MHz} \cdot (1 + R \times 10^{-6}) \tag{2.16}$$

All parameters are floating except for the extra terms in $\omega_{cbo}(t)$ (except ω_0) and τ_{cbo} as described above. The individual calorimeters use the same fit function, except with

$$f(t) = N_{cbo}(t) \cdot N_{2cbo}(t) \cdot (1 + A \cdot A_{cbo}(t) \cdot \cos(\omega_a t + \phi \cdot \phi_{cbo}(t))), \tag{2.17}$$

where the extra included CBO terms are as described in Section 2.7. In all the fits, ω_a is blinded by some amount of ppm in R, as described in DocDB 11232, with a particular string phrase. Finally, the value of the fit function in each time bin is calculated as the integral of the function over the bin, divided by the bin width.

Chapter 3

Analysis Results

3.1 Pre-corrected and corrected energy and time spectra

Before fitting the data and extracting the $g-2$ frequency, pileup has to be removed. The procedure to do this was detailed in Section 2.5, and the results are shown here. Figure 3.1 shows the constructed pileup time spectrum, for pileup energies above threshold. The pre-corrected and corrected time spectra are not shown because differences are small and hard to see. As shown the pileup is almost completely gone by 300 μs. The exact shape of the pileup time spectra is explained in DocDB 14394, which is in general unimportant as long as it is constructed and subtracted properly. Figure 3.2 shows a comparison between the cluster energies and the constructed pileup energies, where differences in the two spectra are small and can be attributed to pileup contamination in the shadow method and triplets which have not been included in this analysis. Figures 3.3, 3.4, and 3.5 show the pre-corrected and corrected energy spectra for the added histograms and for some individual calorimeters. Since the pileup energies are not perfectly reconstructed the corrected energy spectrum does not converge to 0 at the end of the high energy tail, which is readily seen in the log-scale plots. This is okay for the level of statistics included in both the 60H dataset and in Run 1. Systematic effects from getting the pileup amplitude or shape wrong are explored in Section 4.2.

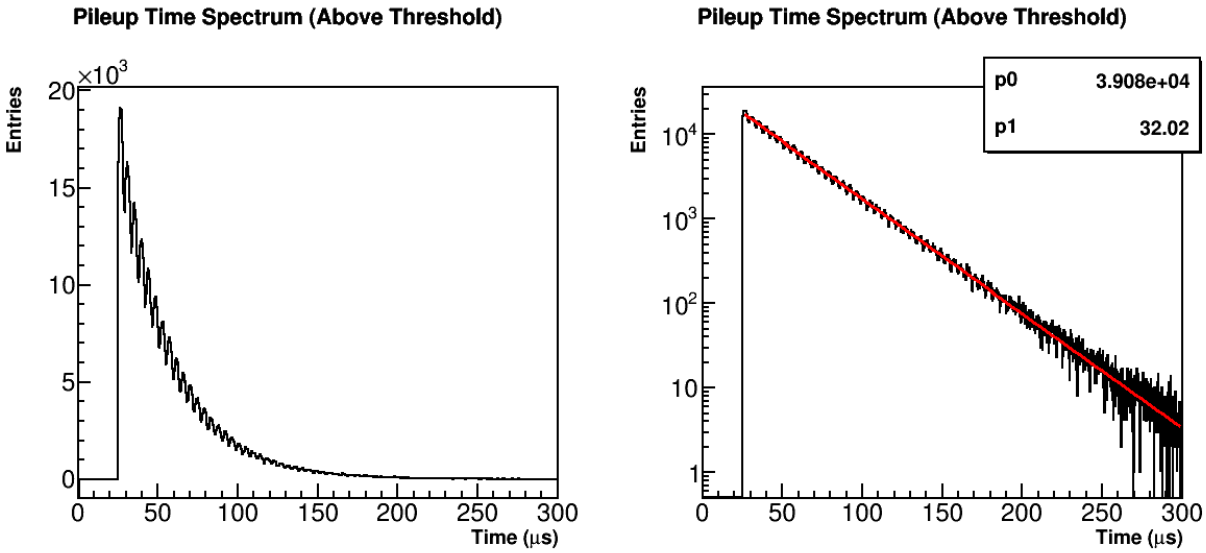

Figure 3.1: Plotted is constructed pileup time spectrum on a linear (left) and log (right) scale. The histogram on the right is fit to a simple two parameter exponential to get an idea of the lifetime of the pileup, calculated here as $32.02\,\mu$s, which is close to half of the muon lifetime at about $64.4\,\mu$s. Reasons for why these two values don't equal include the absence of triplets, lost muons, and an improper fitting function.

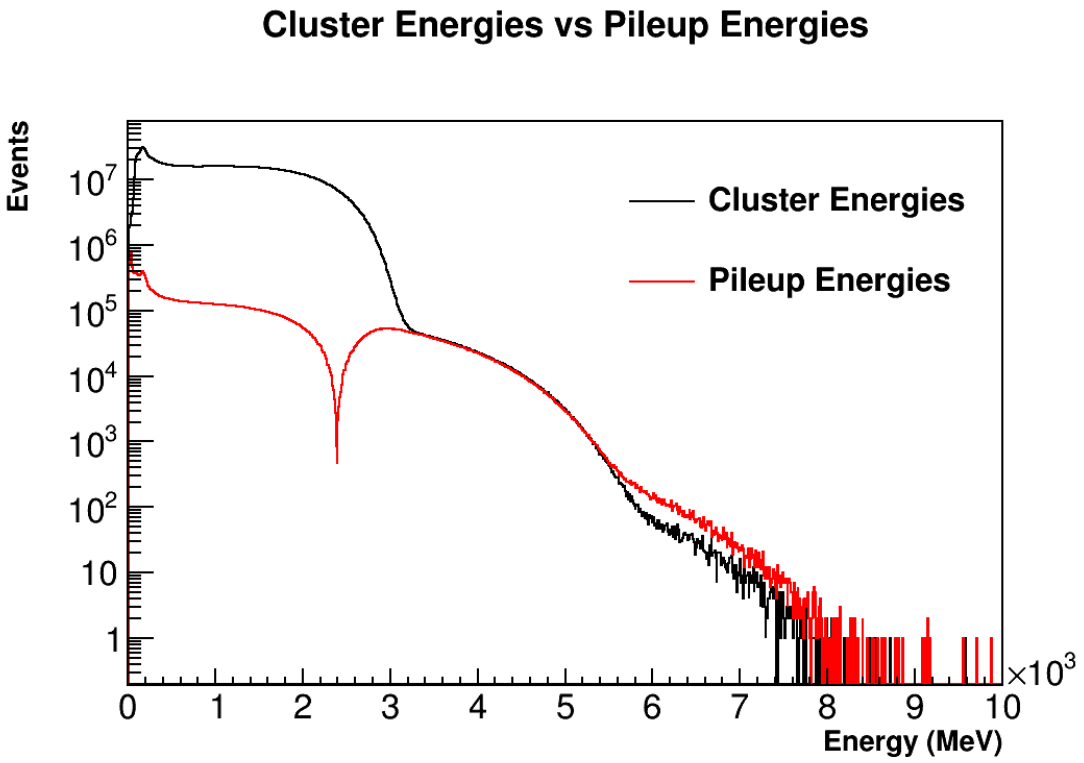

Figure 3.2: Cluster energies in black are plotted vs pileup energies in red, for all calorimeters added together. At energies below about 2.4 GeV the pileup spectrum goes negative. In this plot the absolute value of the pileup energies is plotted, and a spike at about 2.4 GeV can be seen as a consequence of this.

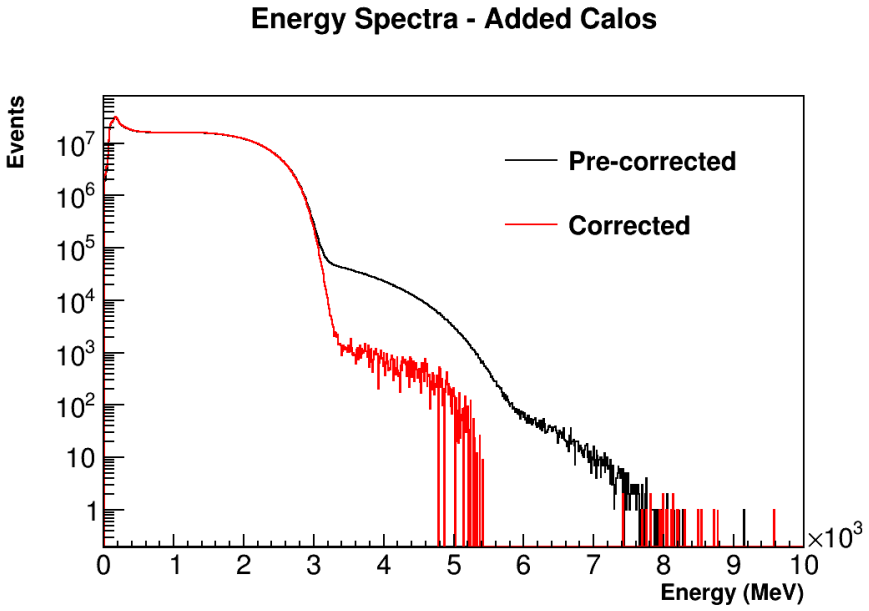

(a) Log scale - the corrected energy spectrum goes negative around 5 GeV.

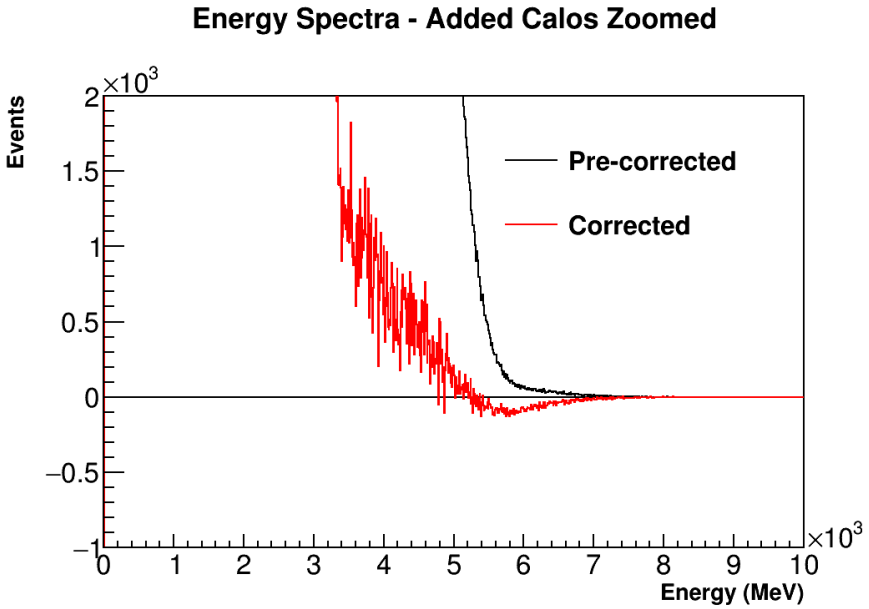

(b) Linear scale - zoomed in to show the shape.

Figure 3.3: Plots for the pre-corrected and corrected energy spectra are shown, all calorimeters added together. Because the triplets and contamination are not accounted for, the corrected energy spectrum does not lie exactly along zero.

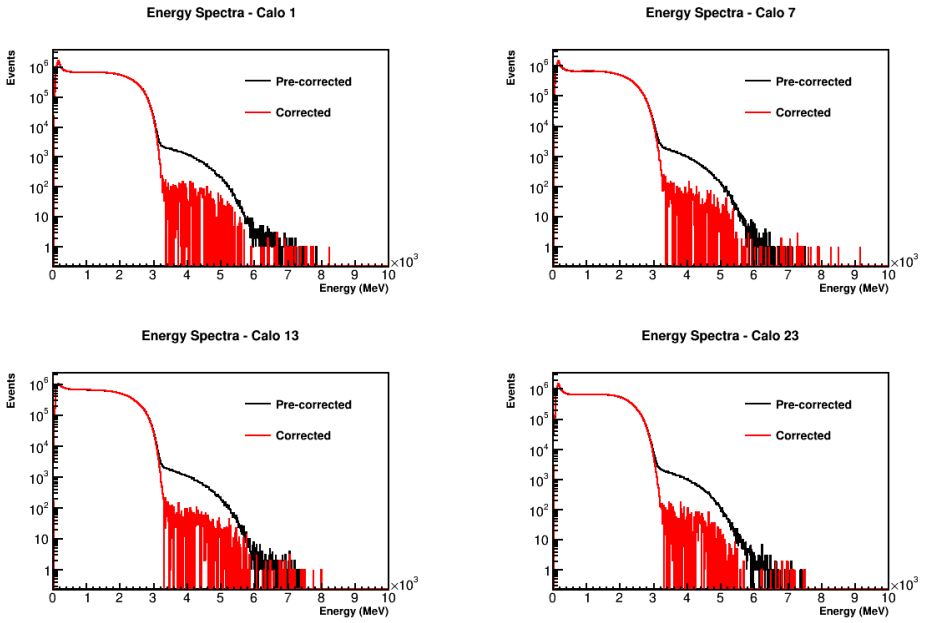

Figure 3.4: Pre-corrected and corrected energy spectra for calorimeters 1, 7, 13, and 23 plotted on a log scale.

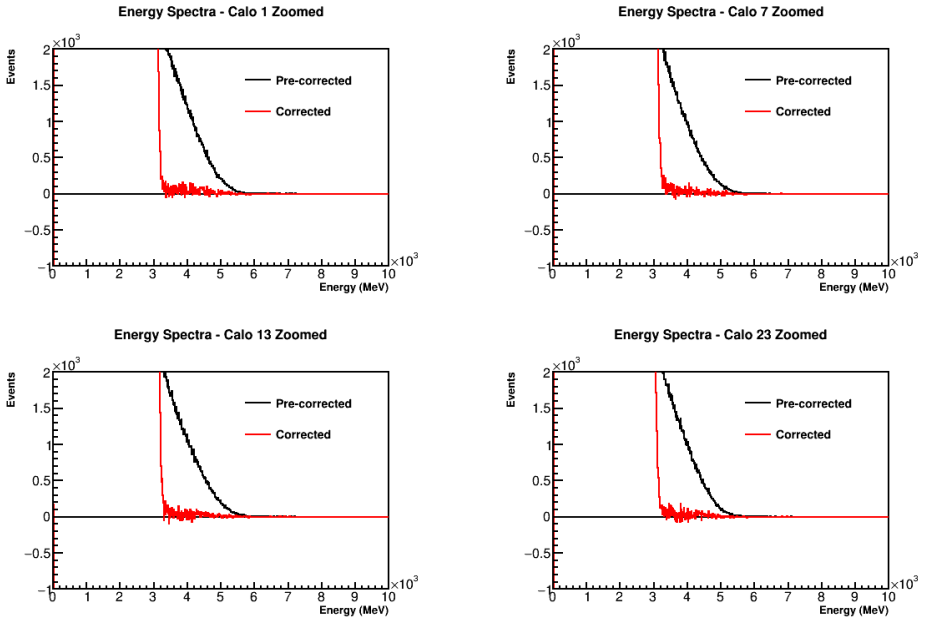

Figure 3.5: Pre-corrected and corrected energy spectra for calorimeters 1, 7, 13, and 23 plotted on a linear scale and zoomed in.

3.2 7 Parameter Ratio Fit

The data has been fit to a 7 parameter function, as described in Section 2.9, reduced from the conventional 14 parameters in a T Method fit. The results are shown in Figure 3.6, with the fit parameters transcribed into Table 3.1. These 7 parameters include the asymmetry "A", the ppm level shift in the $g-2$ frequency "R", the $g-2$ phase "ϕ", and then 4 CBO parameters. As detailed in Section 2.7, these CBO parameters include the frequency "ω_{cbo}", lifetime "τ_{cbo}", and then the CBO amplitude and phase on the N term, "N_{cbo-A}" and "$N_{cbo-\phi}$" respectively. The CBO lifetime has been fixed in the fit to 180 μs. The N and muon lifetime terms are unecessary because the ratio method removes those terms in the data to be fit. The ratio method also divides out slow effects, which removes the need to fit for muon losses. The lack of a low frequency rise in the FFTs of the residuals as shown in Figure 3.9 justifies excluding this term. Finally, due to the specific n value used in gathering the 60H data, the vertical waist (VW) frequency just so happens to be very nearly 10 times the $g-2$ frequency. As described in Section 2.8 this means that the VW does not need to be included in the fit. Like the lost muons this is justified by the lack of a VW peak in the FFT of the residuals. Finally, the fit range is restricted from 30 μs $-$ 500 μs. The early time cut is determined due the instability of the stored muon beam at early times. The late time cut was chosen to avoid the region where the ratio actually starts to widen due to low stats. (This can actually be extended beyond 500 μs safely but that was the limit used by default for previous datasets, and was left in when analyzing the 60H dataset. How far it should be extended is yet to be decided.)

Table 3.2 shows the correlation matrix for the fit parameters in the added calorimeter fit. Figure 3.7 shows the same information in graphical format. As seen the only significant correlation to R is the $g-2$ phase. This is good because it means that if other fit parameters are for some reason fitted slightly incorrectly, the resulting effect on R will be minimal.

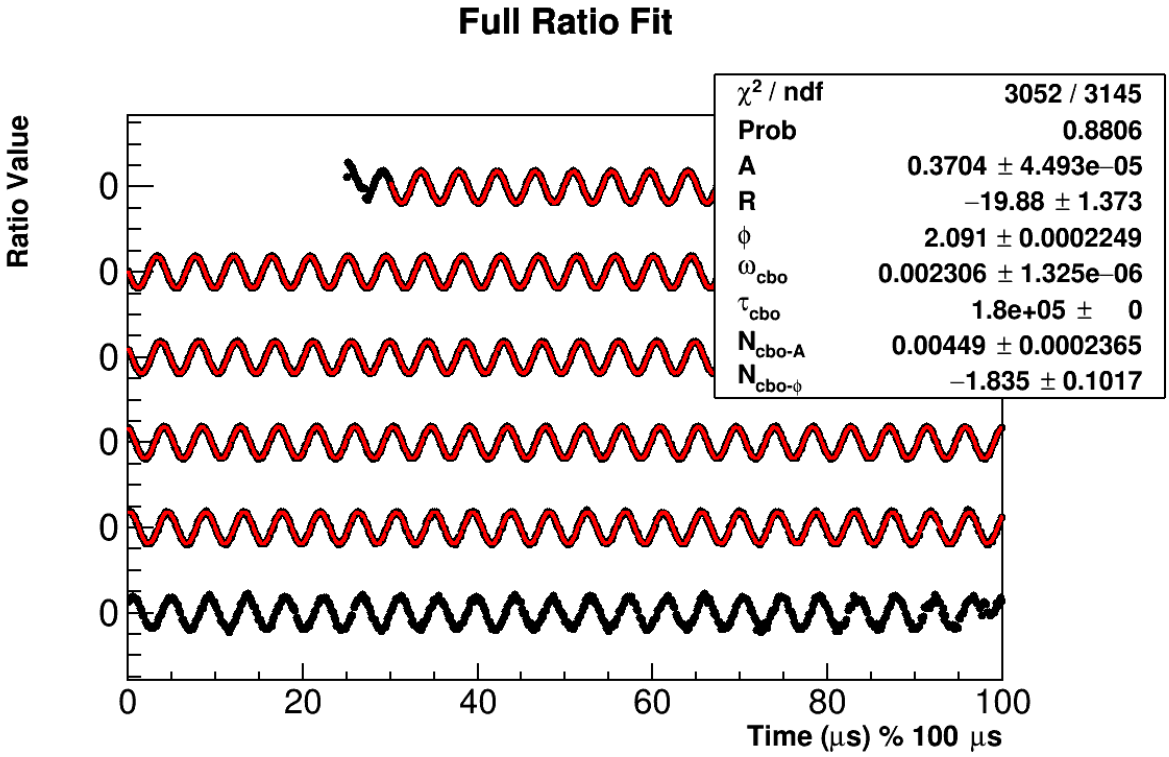

Figure 3.6: Final fit result for the 60 hour dataset. The fit includes 6 free parameters and one fixed. The x axis is in units of μs modulo 100 μs, with successive portions of the data points and fit shifted downwards on the plot. The parameter values in the stats box for the CBO frequency and lifetime are in units of ns. R is blinded locally. The fit ranges from 30 μs to 500 μs.

Fit Results			
χ^2/NDF		3052/3145	
P value		0.8806	
Parameter	Descriptor	Value	Error
A	Asymmetry	0.3704	4.493×10^{-5}
R	R (ppm, blinded)	-19.88	1.373
ϕ	$g-2$ Phase	2.091	2.249×10^{-4}
ω_{cbo}	CBO Frequency (ns^{-1})	0.002306	1.325×10^{-6}
τ_{cbo} (fixed)	CBO Lifetime (μs)	180	0
N_{cbo-A}	CBO N Amplitude	0.00449	2.365×10^{-4}
$N_{cbo-\phi}$	CBO N Phase	-1.835	0.1017

Table 3.1: Table of final fit results.

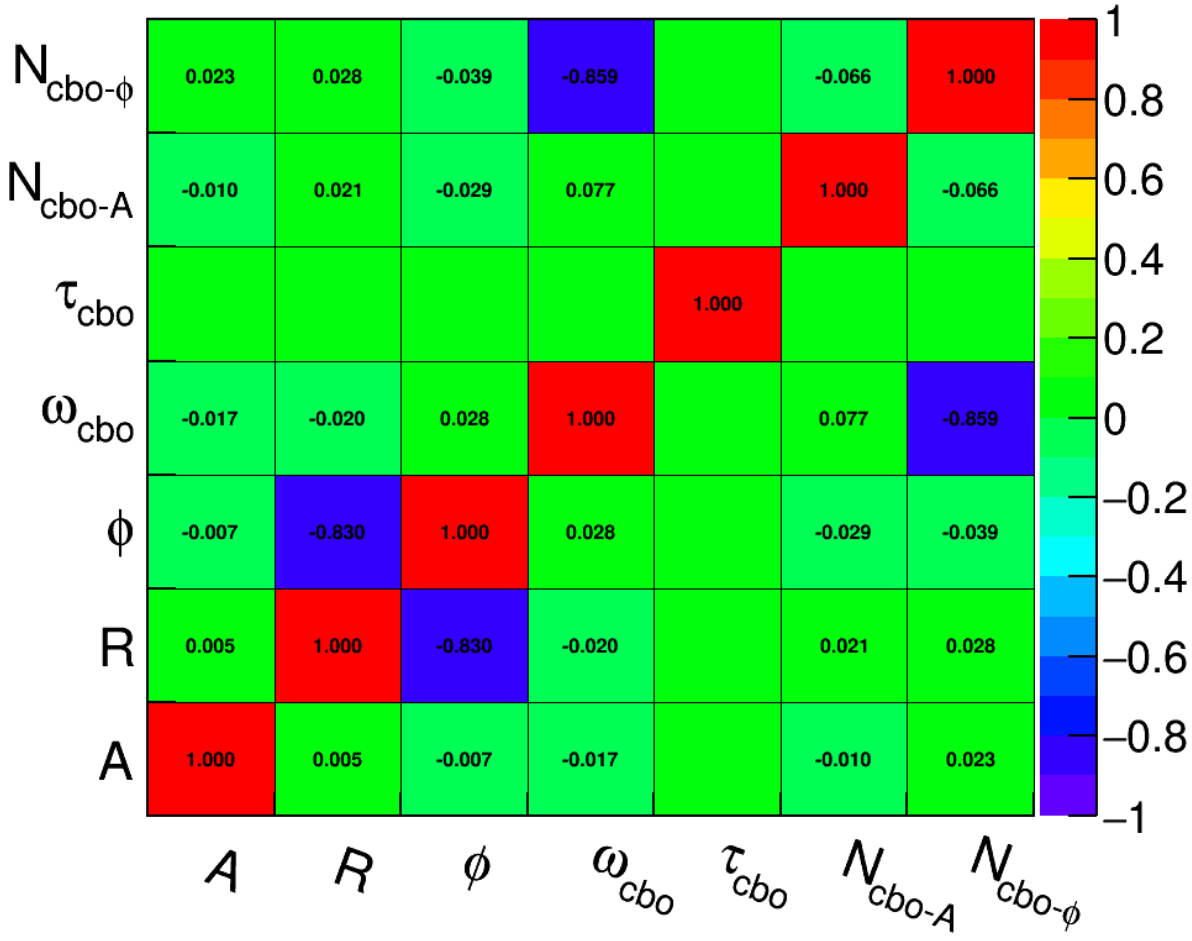

Figure 3.7: Plotted are the correlations between the different fit parameters. Correlations to R are minimal for all fit parameters except the $g-2$ phase. The correlation between the CBO frequency and phase is also easily noticed in this plot.

	A	R	ϕ	ω_{cbo}	τ_{cbo} (fixed)	N_{cbo-A}	$N_{cbo-\phi}$
A	1.0000	**0.0049**	−0.0068	−0.0166	0.0000	−0.0098	0.0233
R	0.0049	**1.0000**	−0.8300	−0.0204	0.0000	0.0207	0.0282
ϕ	−0.0068	**−0.8300**	1.0000	0.0280	0.0000	−0.0287	−0.0387
ω_{cbo}	−0.0166	**−0.0204**	0.0280	1.0000	0.0000	0.0773	−0.8585
τ_{cbo} (fixed)	0.0000	**0.0000**	0.0000	0.0000	1.0000	0.0000	0.0000
N_{cbo-A}	−0.0098	**0.0207**	−0.0287	0.0773	0.0000	1.0000	−0.0656
$N_{cbo-\phi}$	0.0233	**0.0282**	−0.0387	−0.8585	0.0000	−0.0656	1.0000

Table 3.2: Correlation matrix for the full ratio fit. The CBO lifetime is fixed but included in this table. The only significant correlation to R is the $g-2$ phase.

3.3 Residual and FFT

In order to examine the goodness-of-fit, the residuals and the FFT of the residuals need to be examined. The residuals as well as the pulls are shown in Figure 3.8. Also included is a plot of the pulls projected down onto the Y axis. In all three plots no substructure is immediately obvious, and in the latter the pull plot can be seen to have a mean consistent with 0 and an RMS consistent with 1, preliminarily indicating that the fit is good. Plotted in Figure 3.9 is the FFT of the residuals. As can be seen no physical frequencies are observable above the noise. This shows that the CBO has been fitted correctly, and justifies the lack of a muon losses or vertical waist term in the fit. Figure 3.10 shows a similar plot, but this time overlayed with the FFT of the fit residuals for a 5 parameter fit. As seen the CBO, VW, $g-2$, and their beat frequencies, as well as the lost muon peak at low frequencies are removed when performing the full ratio fit.

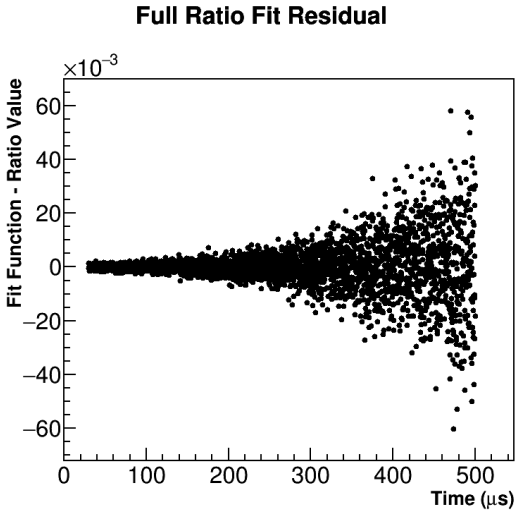

(a) Fit residuals.

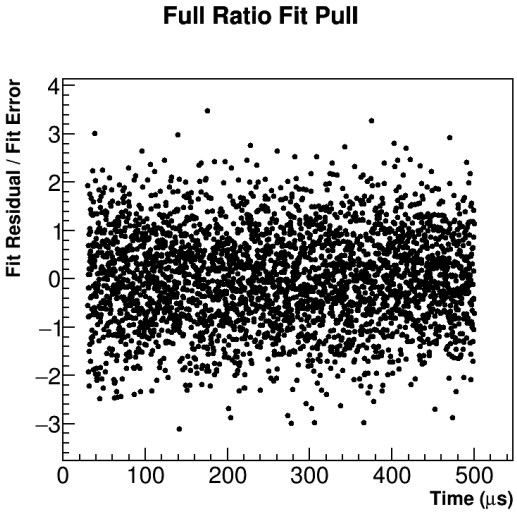

(b) Fit pulls.

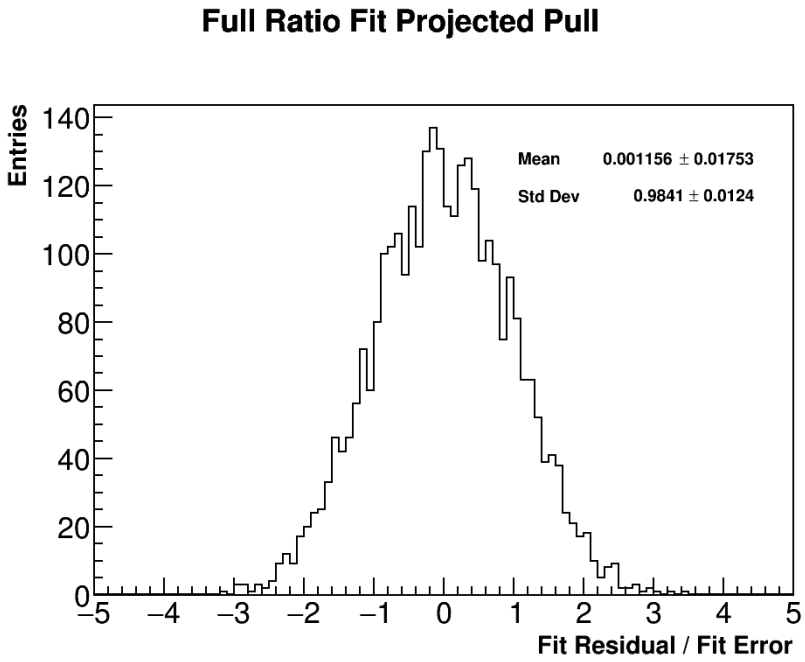

(c) Fit pulls projected onto the y axis. Note the Gaussian shape centered around 0 with unit width.

Figure 3.8: Residuals and pulls for the full ratio fit.

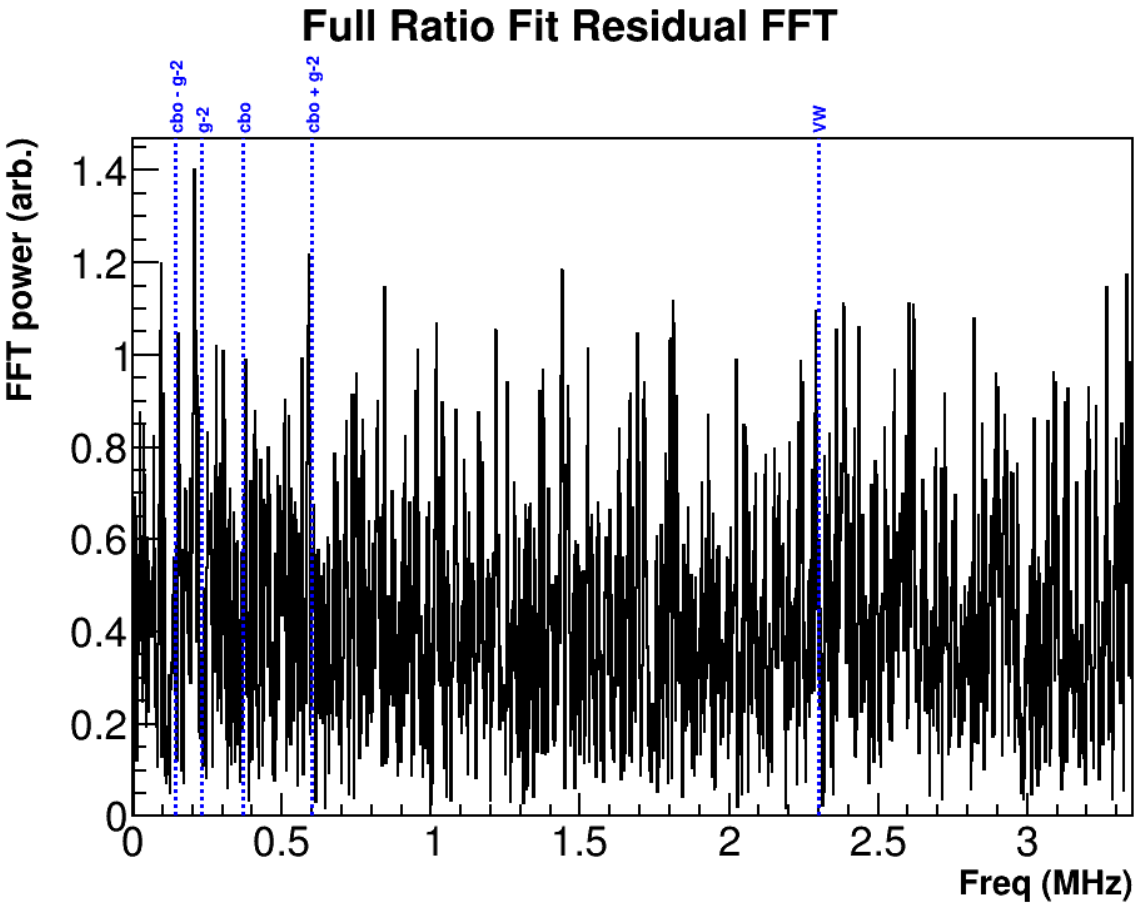

Figure 3.9: FFT of the residuals of the full ratio fit. No significant peaks remain in the ratio fit residuals after fitting with CBO terms. Overlayed are dotted lines for the $g-2$, CBO, and vertical waist frequencies. Peaks close to the lines are coincidental but don't line up when zoomed in.

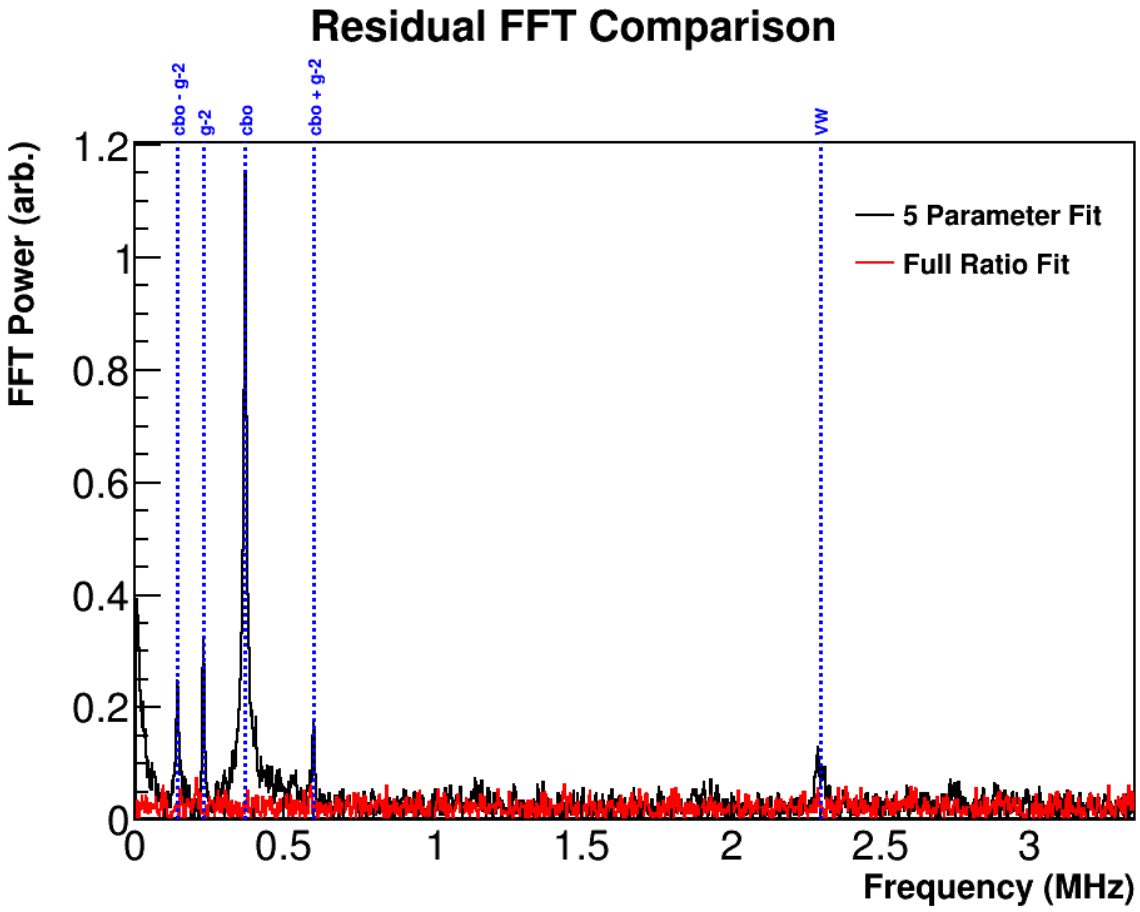

Figure 3.10: A plot of the FFT of the residuals of the fit for the five parameter fit compared to the ratio fit. In black is the FFT for a five parameter fit, where peaks for the CBO and vertical waist can be seen as well as the $g-2$ peak. In red is the FFT of the full ratio fit residuals, where it has been scaled up to be visible on this plot.

3.4 Start time scans

Also necessary to determine whether the fit has been performed appropriately, is to perform start time scans. This procedure involves changing the start bound of the fit as a function of time, and making sure that fit results are consistent. If effects in the data are not properly accounted for, then fit parameters or the goodness-of-fit will change over time and will wander far outside the statistical limits defined by the reduction in data that is fitted. An example of this is shown in Section 4.4.1, where the CBO freqency was originally modelled incorrectly. For the full ratio fit it turns out that this is the only effect that has a negative impact on the fit vs fit start time. As shown in Figure 3.11 the goodness-of-fit is consistent over time, only wandering outside the statistical bands slightly. (This is also partly due to the randomization as mentioned in Section 4.6.4.) Similarly Figure 3.12 shows fit start time scans for each free parameter in the fit. All fit parameters lie comfortably within the statistical bands and are stable vs fit start time, indicating again that the fit is behaving properly.

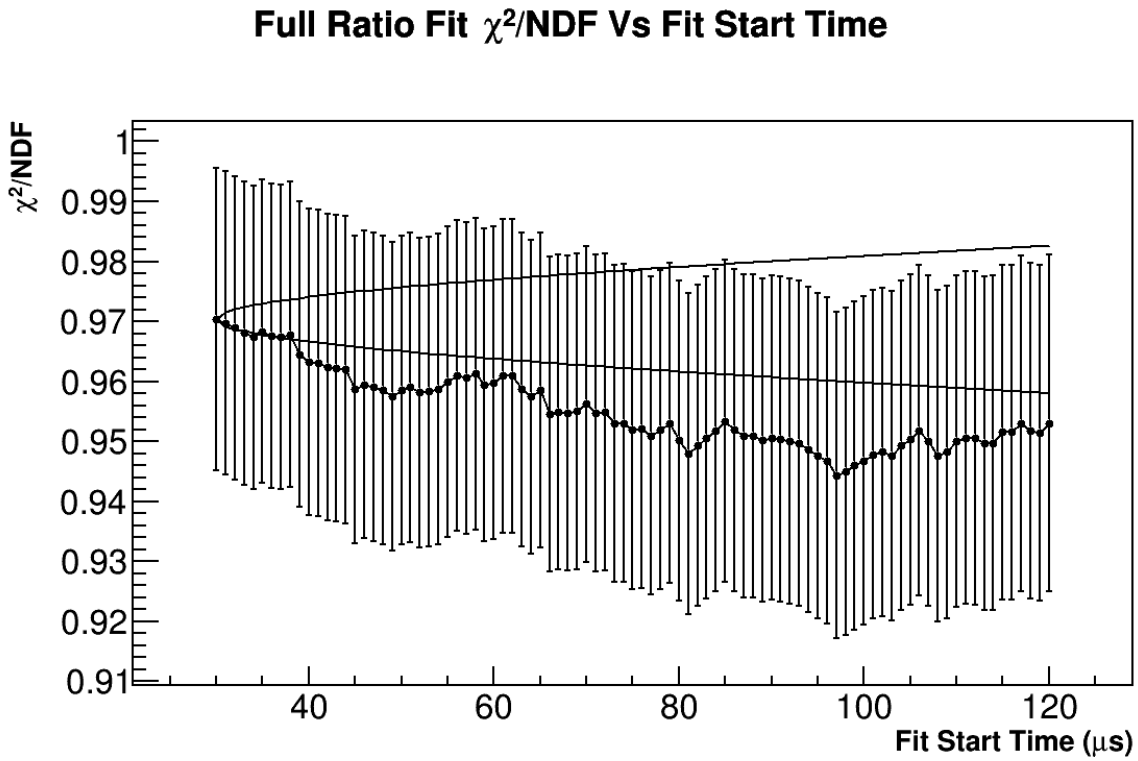

Figure 3.11: Plotted is the χ^2 per degree of freedom vs the start time of the fit. The solid lines indicate the one sigma statistically allowed difference in the fit result coming from the reduction in the data included in the fit. The error bars on the points are calculated as $\sqrt{2/NDF}$.

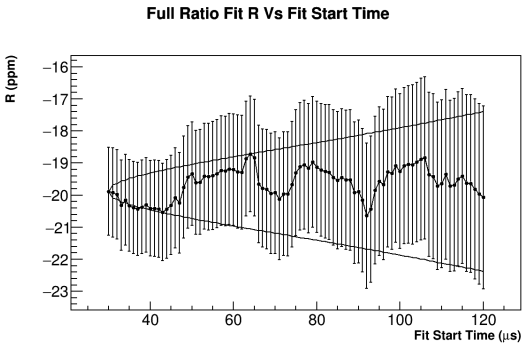

(a) Fitted R value vs fit start time.

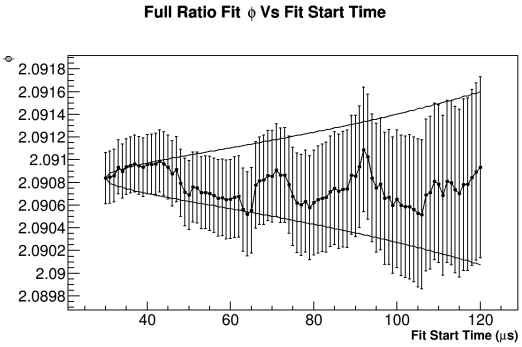

(b) Fitted $g-2$ phase vs fit start time.

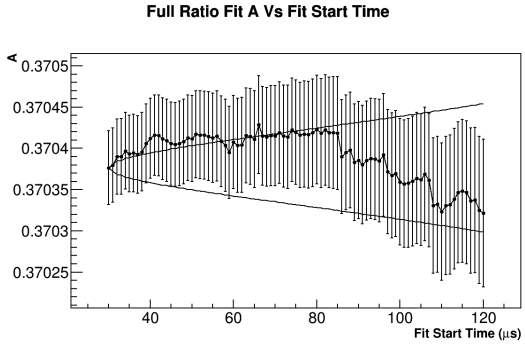

(c) Fitted asymmetry vs fit start time.

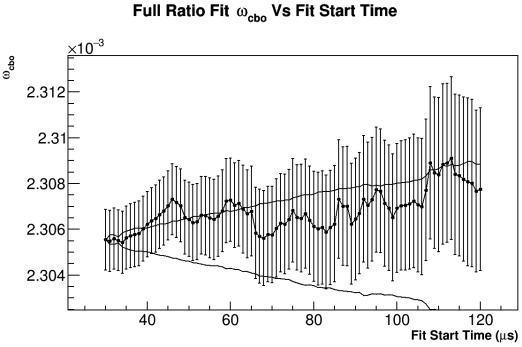

(d) Fitted CBO frequency (ω_0) vs fit start time.

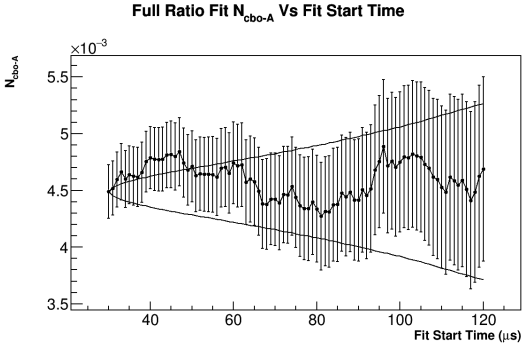

(e) Fitted CBO amplitdue vs fit start time.

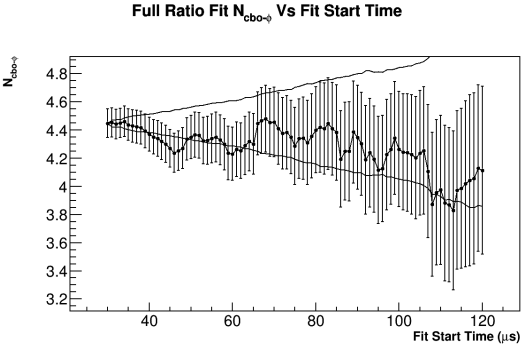

(f) Fitted CBO phase vs fit start time.

Figure 3.12: Start time scans for the free parameters in the full ratio fit. All parameters are consistently within the one sigma statistical bands.

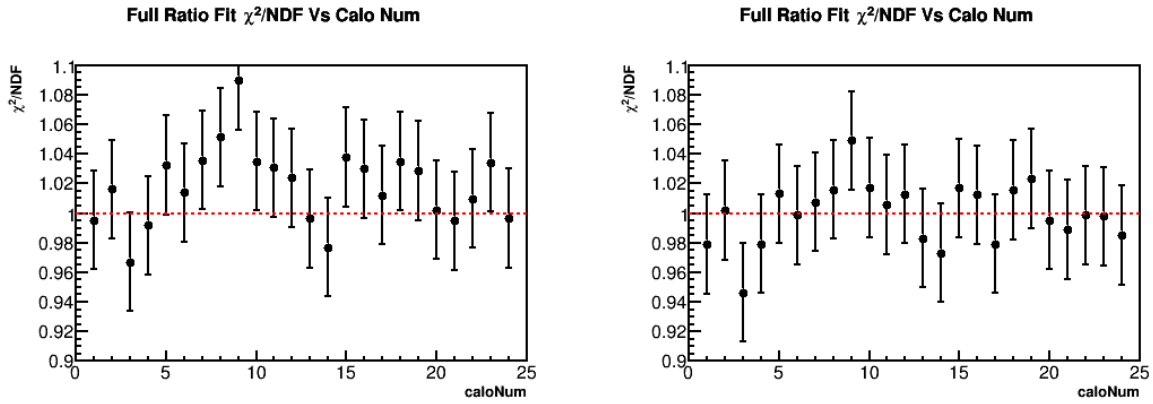

(a) No extra CBO terms, note how most values lie above 1.

(b) Including the extra CBO terms, the results are more or less centered around 1.

Figure 3.13: Plotted is the χ^2 per degree of freedom vs calorimeter number. On the left are the fit results without the extra CBO terms, and on the right are the fit results with them.

3.5 Results vs calorimeter

Finally results are examined on a per calorimeter basis. While there will be some differences in fit results due to the differing acceptance between the calorimeters, in general the results should be consistent. Because of the reduced amount of stats for the individual calorimeters, the fit range has been restricted to 30 - 300 μs as opposed to 30 - 500 μs for the added calorimeter fit. As described briefly in Section 2.7, extra CBO terms are included in the fits, including N_{2cbo}, A_{cbo}, and ϕ_{cbo}. While not all individual calorimeters need all of these terms for good fits, some have poor χ^2 's without them, as shown in Figure 3.13. The fitted parameter results for individual calorimeters are shown in Figures 3.14 and 3.15, where the latter shows fit convergence for the extra CBO parameters. In only a few calorimeters are the extra CBO parameters potentially omittable, as evidenced by larger error bars on the fitted parameters. As seen all calorimeter fits and their parameters behave well.

Of interest to note, calorimeters 13 and 19 have their $g-2$ phases converge to values similar to each other and separate from the rest of the calorimeters, as shown in Figure 3.14b. There is also potentially a slight bump between calorimeters 1 and 24. This behaviour is matched by high N_{cbo} amplitudes shown in Figure 3.14e, and bumps in the N_{cbo} phase shown in Figure 3.14f at the same locations. These calorimeters lie behind the two tracker stations, as well as the empty tracker station near calorimeters 1 and 24. Presumably the different amount of material upstream of these calorimeters leads to a different acceptance and subsequent CBO parameters, which tie into the $g-2$ phase. It's good to see that the fitted R values for these calorimeters are not significantly different in any way. It would be interesting to see if the behaviour of these fitted parameters is reflected in simulation.

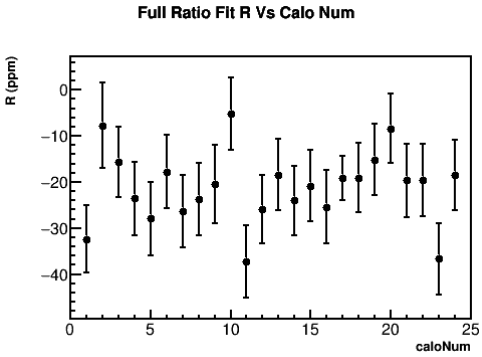

(a) Fitted R value vs calorimeter number.

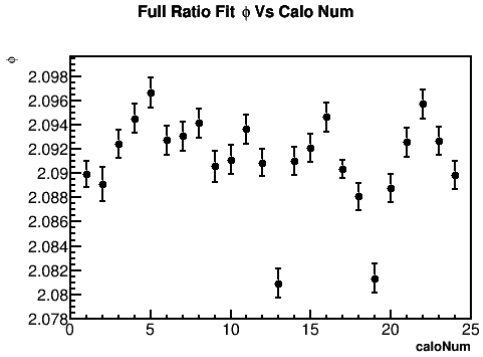

(b) Fitted $g-2$ phase vs calorimeter number. Calorimeters 13 and 19 lie behind the trackers.

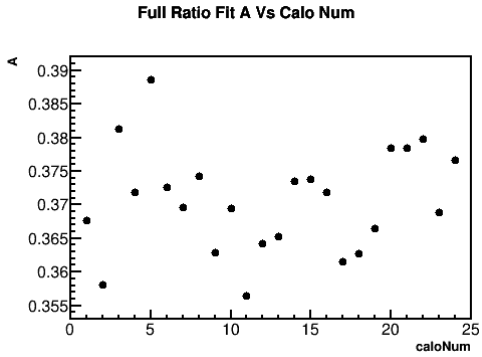

(c) Fitted asymmetry vs calorimeter number.

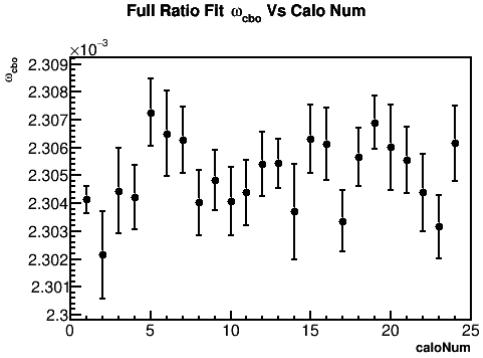

(d) Fitted CBO frequency (ω_0) vs calorimeter number.

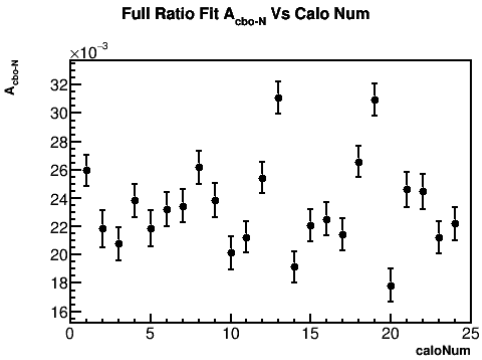

(e) Fitted CBO amplitdue on the N parameter vs calorimeter number.

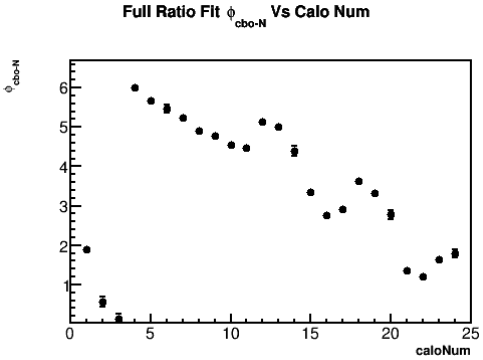

(f) Fitted CBO phase on the N parameter vs calorimeter number. The CBO phase varies from 0 to 2π around the ring.

Figure 3.14: Full ratio fit parameter values vs calorimeter number.

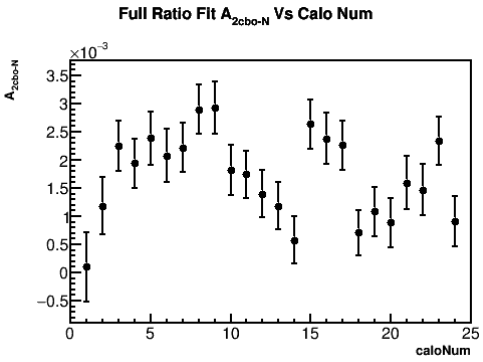

(a) Fitted CBO amplitdue on the N parameter for twice the CBO frequency vs calorimeter number.

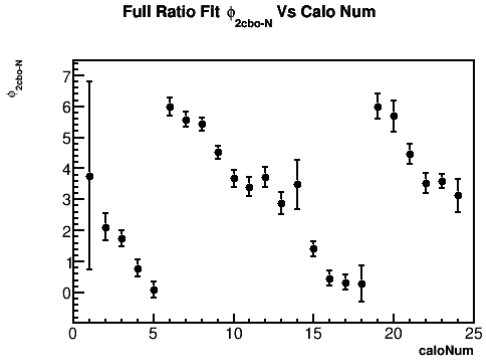

(b) Fitted CBO phase on the N parameter for twice the CBO frequency vs calorimeter number.

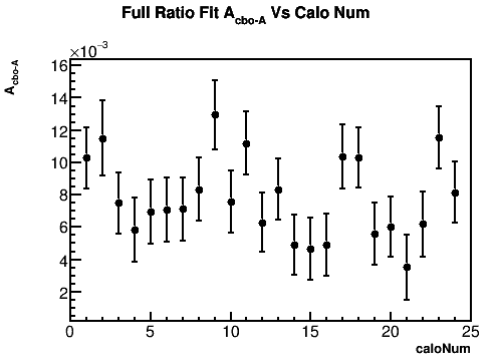

(c) Fitted CBO amplitdue on the A parameter vs calorimeter number.

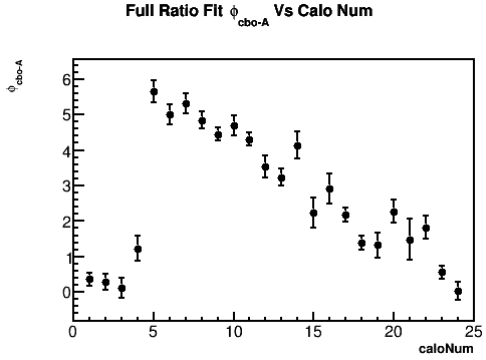

(d) Fitted CBO phase on the A parameter vs calorimeter number.

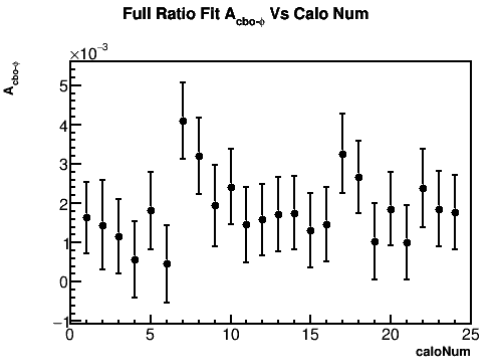

(e) Fitted CBO amplitdue on the $g-2$ phase parameter vs calorimeter number.

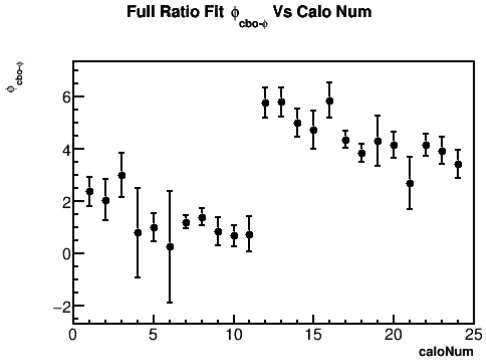

(f) Fitted CBO phase on the $g-2$ phase parameter vs calorimeter number.

Figure 3.15: Full ratio fit parameter values vs calorimeter number. Plotted here are the extra CBO parameters which improve most single calorimeter fits. In each CBO phase parameter, the phase varies from 0 to 2π around the ring, except for the N_{2cbo} term where it wraps around twice.

Chapter 4

Systematic Uncertainty Evaluations

4.1 Sensitivity of ω_a to gain corrections

I estimate the systematic error on R due to the the in-fill gain function at 24.8 ppb, and to the Short Term Double Pulse correction at blank ppb. Adding these in quadrature results in a systematic error of blank ppb.

4.1.1 In-Fill Gain

As positrons hit the calorimeters throughout the fill, there will be a gain sag response such that the energy of detected positrons changes throughout the fill, dropping at first and then rising exponentially back up to their true values. This changing energy response will lead to a systematic error on R, as positrons with mis-measured energies near the energy threshold are excluded from the fit. This gain sag is corrected for in the Recon West code, before I fill my histograms. Due to the way I've constructed my analysis code, it's not so simple to modify the reconstruction code and create new histograms quickly. Such a process would require the rebuilding of many sets of new cluster root trees, and then making histograms from those. As a faster way of getting at the in fill gain systematic error, I've instead chosen to apply a gain sag function to the incoming energy-corrected clusters. This allows me to scan over gain sag function parameters and only run off one set of trees, as I've been doing for all systematic studies.

(Should this bit be in the analysis procedures chapter?) The in-fill gain sag function was determined by Matthias Smith and the laser team as shown in DocDB 14077. (Cite or link?) The function goes as

$$E = E_0(1 - A \cdot e^{-(t-t_{offset})/\tau}), \tag{4.1}$$

where E_0 is the orginal energy of the positron cluster, A is the amplitude factor on the gain sag function, τ the lifetime, and then t_{offset} the shift of the function from 0. It is this function that is inverted and applied to the clusters in the reconstruction. I apply a function of the same form in my own code before filling hits into histograms, in essence undoing the reconstruction gain correction as a way to measure the in-fill gain sag effect on R.

There are some simplifications and assumptions I've made when applying said gain sag function in my own code. First is that while in the reconstruction code each crystal of each calorimeter has its own singular in-fill gain function, one of which is shown in Figure 4.1, I apply a global gain sag function to all incoming clusters. Secondly the default parameters

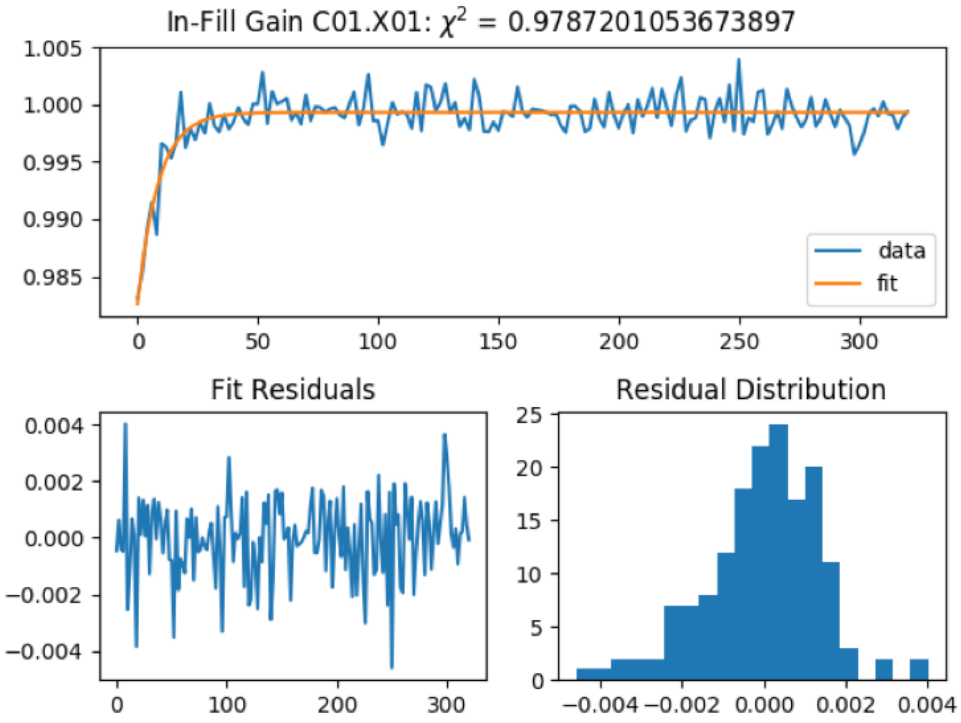

Figure 4.1: The top plot shows the in-fill gain sag function in orange from a fit to data in blue, for crystal 1 in calorimeter 1. The gain sag can be modeled effectively by a simple exponential function. By 30 μs the change in energy response is nearly only .1%. (Might want to look up these exact numbers.) The bottom two plots show the residuals of the fit. Plot made by Matthias Smith.

for the gain sag function are simply eyeballed from the fcl file where all crystal parameters are stored. These values are 0.03 for the amplitude, 6.7 μs for the lifetime, and 3.907 μs for the offset. (Once the latest dataset is available I will need to come up with a better way to apply this gain sag function, either with multiple functions per crystal or with parameters that are actual averages. For now it's fine though to get words on the paper.) Finally, I apply this gain sag function after I apply the artificial deadtime to the incoming clusters, due to code restrictions. This should be a small effect. These assumptions I believe should be okay as long as I take my systematic errors conservatively.

To calculate the systematic error, I simply scan over the gain sag function parameters and observe the changes in R. This includes scans over the amplitude, lifetime, and offset as described in 4.1, and shown in Figure 4.2. I calculate the systematic error on R as the

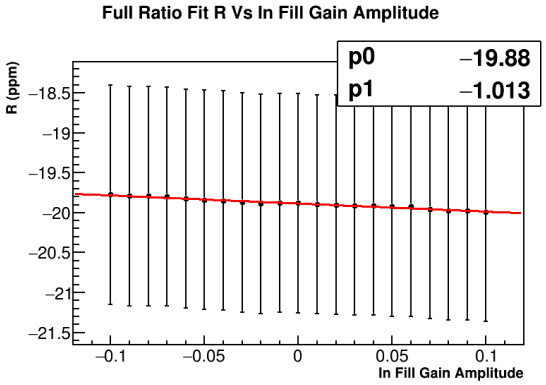

(a) Plotted is R vs the amplitude parameter in the gain sag function. The slope is -1.013 ppm per unit amplitude.

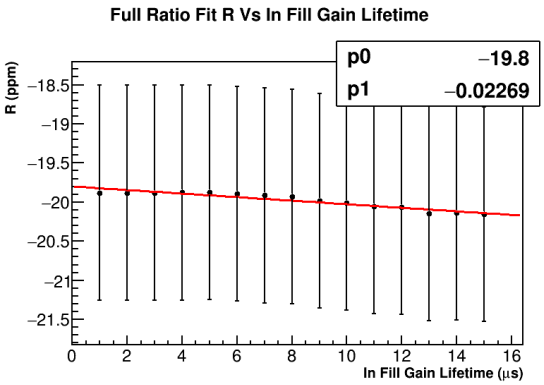

(b) Plotted is R vs the lifetime parameter in the gain sag function. The slope is -0.02269 ppm per μs.

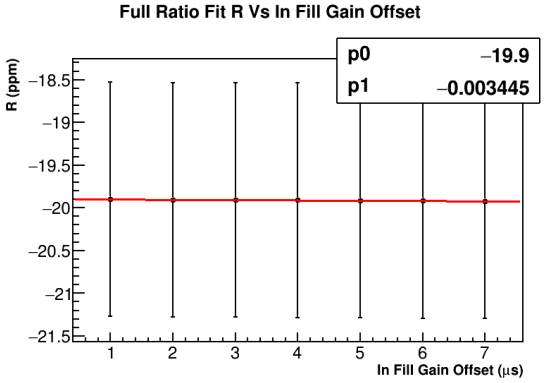

(c) Plotted is R vs the offset parameter in the gain sag function. The slope is -0.0034 ppm per μs.

Figure 4.2: Plotted is fitted R values vs gain sag function parameters. In each case I scanned over ranges approximately centered around the eyeballed average values.

quadrature sum of the separate pieces as

$$\delta R_A = \delta\alpha_A \times \frac{dR}{d\alpha_A}, \tag{4.2}$$

$$\delta R_\tau = \delta\alpha_\tau \times \frac{dR}{d\alpha_\tau}, \tag{4.3}$$

$$\delta R_{offset} = \delta\alpha_{offset} \times \frac{dR}{d\alpha_{offset}}, \tag{4.4}$$

where $\delta\alpha_A$, $\delta\alpha_\tau$, and $\delta\alpha_{offset}$ are the uncertainties on the gain sag amplitude, lifetime, and offset respectively. I take the uncertainty on the amplitude very conservatively at 1%, leading to a systematic error on R of $0.01 \times 1.013\,\text{ppm} = 10.1\,\text{ppb}$. I take the uncertainty on the lifetime very conservatively at $1\,\mu$s, leading to a systematic error on R of $1 \times 22.7\,\text{ppb} = 22.7\,\text{ppb}$. Finally the slope for the offset parameter is very flat, and that combined with a very uniform array of values for the offset parameter in the reconstruction (indicative of a very small uncertainty), means that the systematic error on R is negligible. Therefore I ignore the offset parameter and add the amplitude and lifetime errors in quadrature to produce a systematic error on R of 24.8 ppb. (The uncertainty on the parameters would be the fit errors on the parameter I think, except for the fact that I'm using a global gain sag function as opposed to crystal functions, meaning the uncertainty might be the spread in parameters. I'm not entirely sure. Also I have removed the offset parameter in my latest code and will reproduce these results without it with the new dataset when it's available.)

4.1.2 Short Term Double Pulse (SDTP)

Work and writing to be done here. I plan on reconstructing clusters w/ and w/o the SDTP included and comparing the results to determine the systematic effect on R.

4.2 Sensitivity of ω_a to pileup

The systematic error on R due to the pileup construction consists primarily of two parts, the error due to misconstruction of the amplitude and the phase of the pileup. I estimate the systematic error on R due to the pileup amplitude at 22.6 ppb, and to the pileup phase in pieces of 25.7 and 16.1 ppb. Adding these in quadrature results in a systematic error of 37.8 ppb.

4.2.1 Pileup Amplitude

The error due to the amplitude misconstruction was calculated by scanning over a pileup multiplier parameter, from 90% of the calculated pileup amplitude to 110%, as shown in Figure 4.3. The sensitivity of R to the amplitude was determined to be -509.1 ppb per unit

amplitude. The uncertainty of the pileup amplitude construction was determined by fitting a parabola to the χ^2 as a function of the pileup amplitude, and taking the width of that parabola as the uncertainty. This width is determined as the distance in X for the χ^2 to rise by 1 from the minimum, also calculated as $\sqrt{2/(\chi^2)''}$.

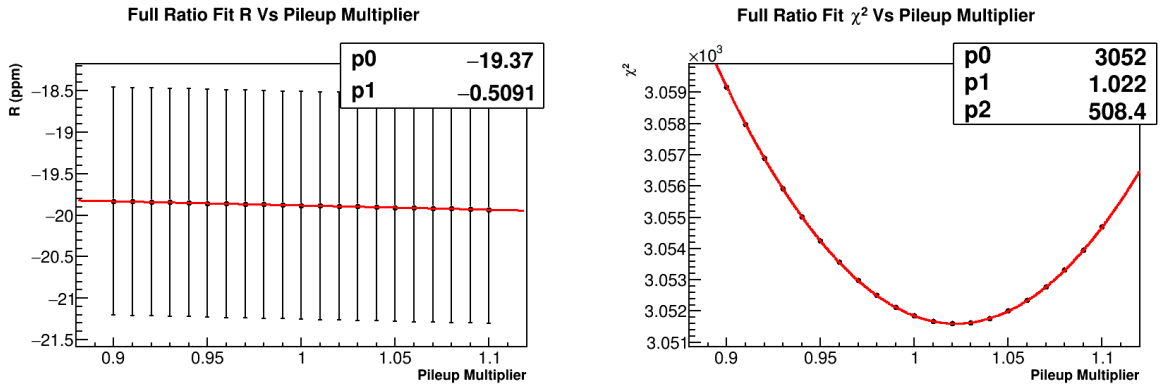

(a) Sensitivity of R vs the pileup amplitude. The slope is -509.1 ppb per unit amplitude.

(b) Plotted is the fitted χ^2 vs the pileup amplitude. The fit equation used was $p2 \times (x - p1)^2 + p0$. The minimum lies at 1.022.

Figure 4.3: The significant plots to determine the pileup amplitude systematic error.

This corresponds to an uncertainty of $\sqrt{1/508.4} = 0.0444$ or 4.44%. The minimum of the χ^2 plot of 1.022 lies at approximately $.5\sigma$ away from 1, which is consistent and nice to see. Then, calculating the systematic error on R due to the pileup amplitude construction as

$$\delta R_{pm} = \delta\alpha_{pm} \times \frac{dR}{d\alpha_{pm}} \tag{4.5}$$

where $\delta\alpha_{pm}$ is the uncertainty on the pileup amplitude, the systematic error on R is calculated as $0.0444 \times 509.1\,\text{ppb} = 22.6\,\text{ppb}$.

Another technique to estimate the uncertainty of the pileup amplitude construction is to look at the offset of the high energy tail of the pileup subtracted energy spectrum from zero. Because however I've applied only the doublet correction, I know that the shape of the pileup spectrum is wrong by some amount, as evidenced in Figure 3.3. While the pileup itself can multiplied by some scaling factor other than 1 in order to align the energy spectra slightly better, because the shape of the pileup correction is imperfect the offset calculation I believe is the wrong way to go about calculating this uncertainty in my case. The shape can be fixed by including the triplets and the doublet contamination in the shadow method, but that work is incomplete. Since the triplets are a 1% effect relative to the doublets, and the contamination is of the same order, I believe the uncertainty of 4.44% conservatively

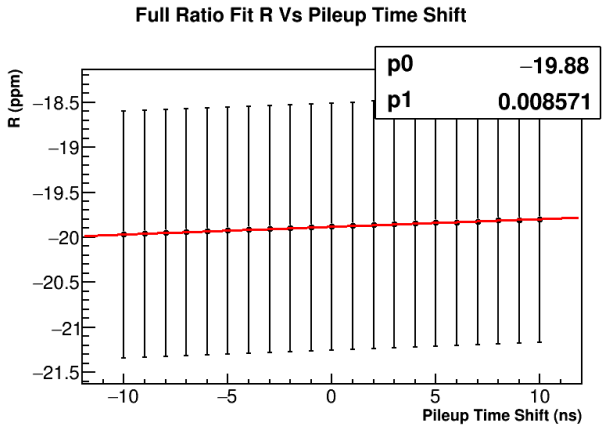

Figure 4.4: Sensitivity of R vs the pileup phase. The slope is 8.571 ppb per ns.

includes for this mismatch in shape and the omission of the triplets. Regardless, since the statistics of the 60H dataset is much larger than the order of the systematic effect for the pileup construction ($\mathcal{O}$(1 ppm) vs $\mathcal{O}$(10 ppb)), this is a fine assumption.

4.2.2 Pileup Phase

The error on R due to the pileup phase construction was calculated by scanning over a pileup time shift parameter, where the pileup spectrum was shifted in time by some amount before subtraction. The sensitivity of R to this parameter is shown in Figure 4.4. It is extremely unlikely that the entire pileup spectrum could be shifted by the offsets shown here, so this is a conservative estimate of the effect of the pileup phase on R. I then calculate the phase error as

$$\delta R_{pp} = \delta\alpha_{pp} \times \frac{dR}{d\alpha_{pp}} \tag{4.6}$$

where $\delta\alpha_{pp}$ is the uncertainty on the pileup phase. Conservatively estimating the uncertainty on the pileup phase as half the artificial deadtime at 3 ns, the systematic error on R is then calculated as $3\,\text{ns} \times 8.571\,\text{ppb/ns} = 25.7\,\text{ppb}$. Figure 4.5 shows the change in R vs fit start times for pileup time shifted spectra vs the unshifted pileup time spectra. As shown the difference converges to zero as the level of pileup diminishes over the course of a fill.

As mentioned in section Section 2.5, the energy of the pileup pulses may not actually be exactly equal to the sum of the pileup singlets. If the energy of the pileup pulses are systematically miscalculated, then doublets will be added or lost near the energy threshold applied when constructing the pileup spectrum. This leads to an additional error on the

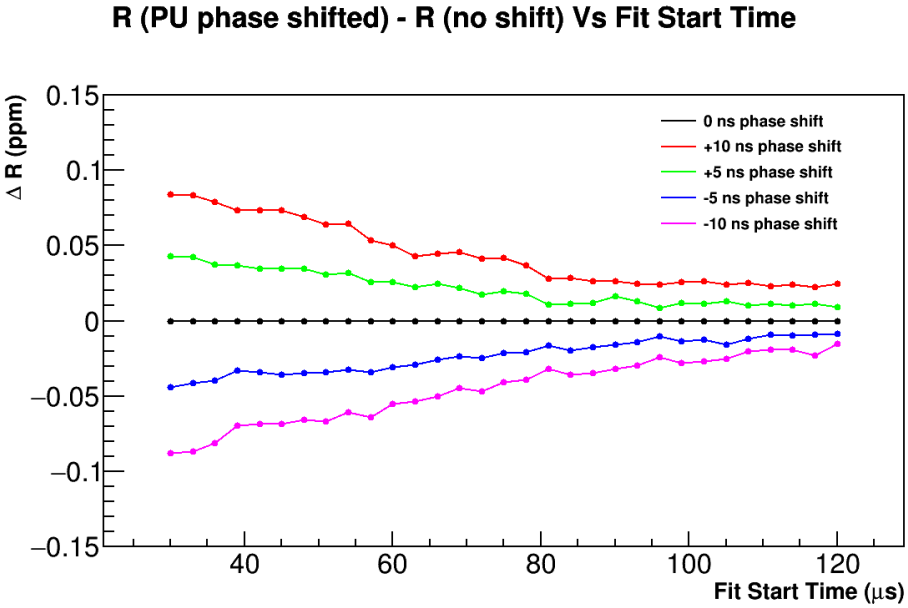

Figure 4.5: Plotted is ΔR between pileup time shifted and unshifted results vs fit start time. The black line and points are by definition 0. As the fit start time increases and the pileup reduces, the ΔR points converge to zero as they should.

phase which needs to be included. With the energy of the pileup pulses calculated as

$$E_{doublet} = C \cdot (E_1 + E_2), \tag{4.7}$$

by scanning over the parameter C this error can be determined. The sensitivity of R to this pileup energy scaling parameter is shown in Figure 4.6, with a slope of -806.5 ppb per unit scaling parameter. The systematic error on R is calculated in the usual way,

$$\delta R_{pe} = \delta \alpha_{pe} \times \frac{dR}{d\alpha_{pe}} \tag{4.8}$$

where $\delta\alpha_{pe}$ is the uncertainty on the pileup energy dependence. This uncertainty was calculated in the same manner as was done for the pileup amplitude, by fitting a parabola to the χ^2 as a function of the energy scaling parameter, and it was determined to be 2%. The systematic error on R is then calculated as $0.02 \times 806.5\,\text{ppb} = 16.1\,\text{ppb}$.

4.3 Sensitivity of ω_a to lost muons

I estimate the systematic error on R due to the lost muon function at 36.1 ppb, and to the lost muon bias as

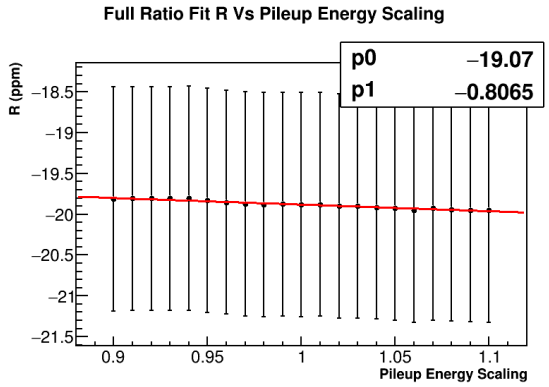

(a) Sensitivity of R vs the pileup energy scaling parameter. The slope is -806.5 ppb per unit energy scaling.

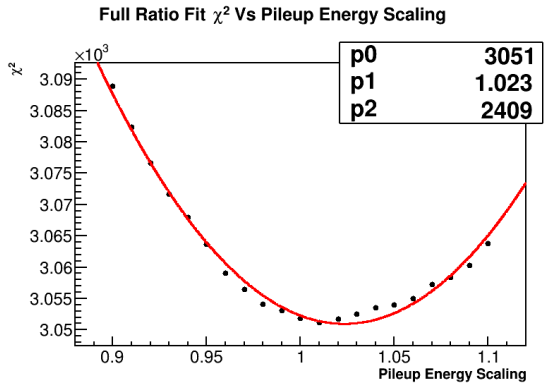

(b) Plotted is the fitted χ^2 vs the pileup energy scaling parameter. The fit equation used was $p2 \times (x - p1)^2 + p0$. The minimum lies at 1.023.

Figure 4.6: The significant plots to determine a part of the pileup phase systematic error.

4.3.1 Lost muon function

As described in Section 2.6, the lost muon function does not need to be included in the ratio fit. In order to calculate a systematic error from excluding the lost muon function, I added the function to the fit as described in that section. I fixed the value of the κ_{loss} parameter to that determined from a T Method fit of the same data. The results can be seen in Figure 4.7. The final fitted R value differs from the non-LM fitted function by -36.1 ppb. Therefore I take the the systematic error from excluding the lost muon function as 36.1 ppb.

4.3.2 Lost muon bias

4.4 Sensitivity of ω_a to CBO function

I estimate the systematic error on R due to the CBO frequency at 30 ppb, to the CBO envelope shape at 21.1 ppb, and to the fixed CBO lifetime at 12.1 ppb. Adding these in quadrature results in a systematic error of 38.6 ppb.

4.4.1 CBO Frequency

As described in Section 2.7, the CBO frequency as a function of time changes over the course of a fill. Shown in Figure 4.8 is a comparison between the fitted CBO frequency parameter as a function of fit start time for a constant frequency vs a changing frequency. Without the changing frequency the fit behaves improperly. Because a specific model was chosen for the CBO frequency, there will be a systematic error on R that needs to be determined. James

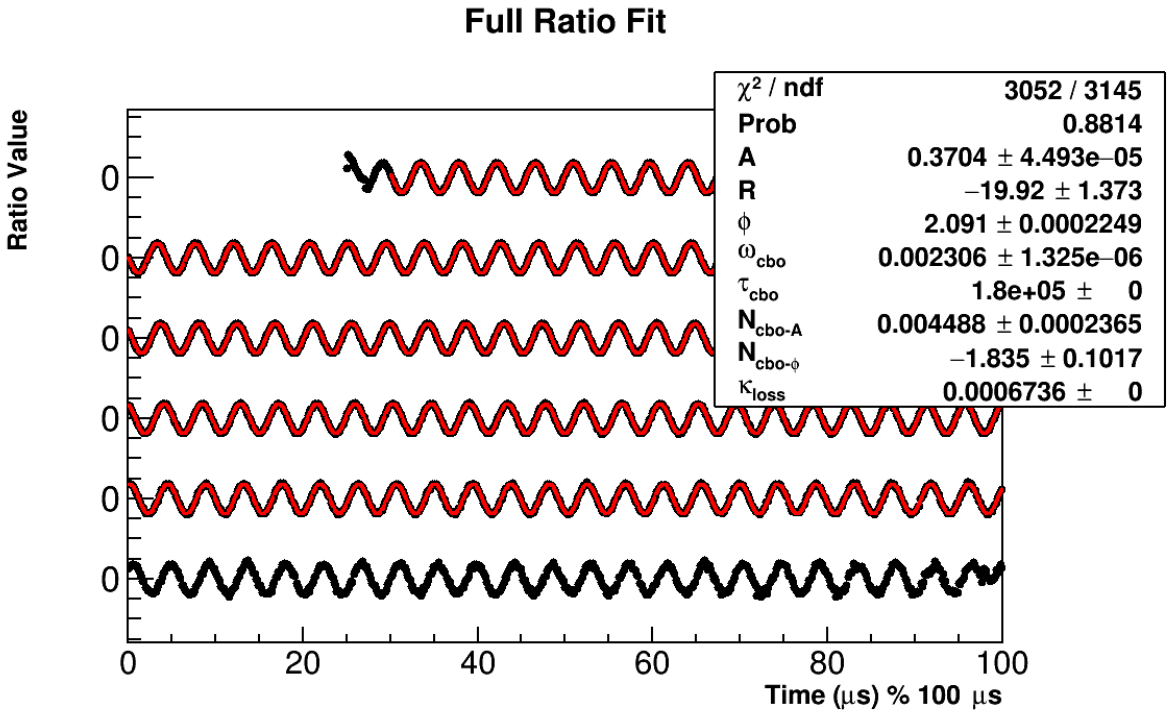

Figure 4.7: Fit results with the LM term included. The lost muon parameter has been fixed. The x axis is in units of μs modulo 100 μs, with successive portions of the data points and fit shifted downwards on the plot. The parameter values in the stats box for the CBO frequency and lifetime are in units of ns. R is blinded locally. The fit ranges from 30 μs to 500 μs.

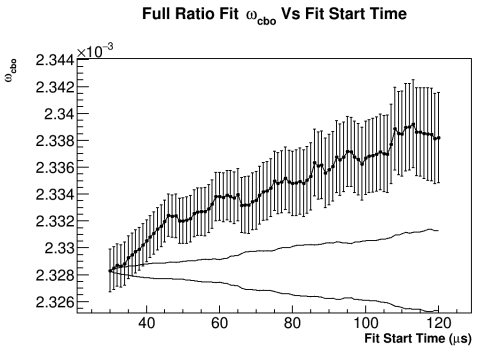

(a) Fixed CBO frequency.

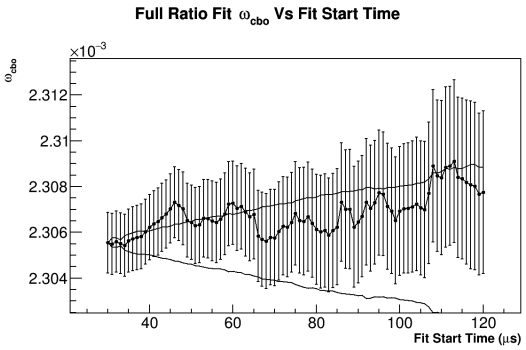

(b) Changing CBO frequency.

Figure 4.8: Fit start time scans for the CBO frequency parameter with a fixed frequency (left) and for the tracker model frequency (right). With the inclusion of the changing frequency over time, the fit parameter becomes stable as a function of fit start time.

Mott examined the frequency function he derived from the data in greater detail in DocDB 15376, where he considered parameter correlations in Equation 2.7 and subsequent effects on the overall function. He found that errors were small, parameters were highly correlated, and that the CBO frequency function was very well constrained, as well as comparable between stations 12 and 18, and the 60H and 9d datasets.

In order to determine the systematic error on R, I simply varied the individual fixed parameters in the CBO frequency function $\{\Delta\omega, A, \tau_A, B, \tau_B\}$, by $\pm 2\sigma$, where the errors on the parameters were taken from DocDB 15376. I also fit the data with the station 18 parameters. Even though the frequency parameters are highly correlated, varying them individually should be a conservative method for determining the overall systematic error on R. I found a 25 ppb difference in the fitted R value for the station 18 parameters, as compared to the station 12 parameters, primarily due to the different "A" value, and differences of order 5 ppb or less for the rest of the parameters. Adding them in quadrature resulted in an error of approximately 27.3 ppb. In order to be slightly more conservative, I estimate the systematic error on R due to the frequency at 30 ppb.

4.4.2 CBO Shape

If the shape of the CBO in the fit function is wrong, then there will be a systematic error on R. Because I get good fits and the CBO parameters are stable vs fit start time, the possbile changes to the envelope are limited, compared to the envelope used as shown in Equation 2.8. Possible changes to the envelope include those functions as shown in Figure 4.9, an exponential plus a constant and then an exponential times another oscillatory term. Both new envelopes were determined from tracker analysis fits to the CBO amplitude. Both changes to the envelope amplitude were tried in the fitting function, with changes in R of

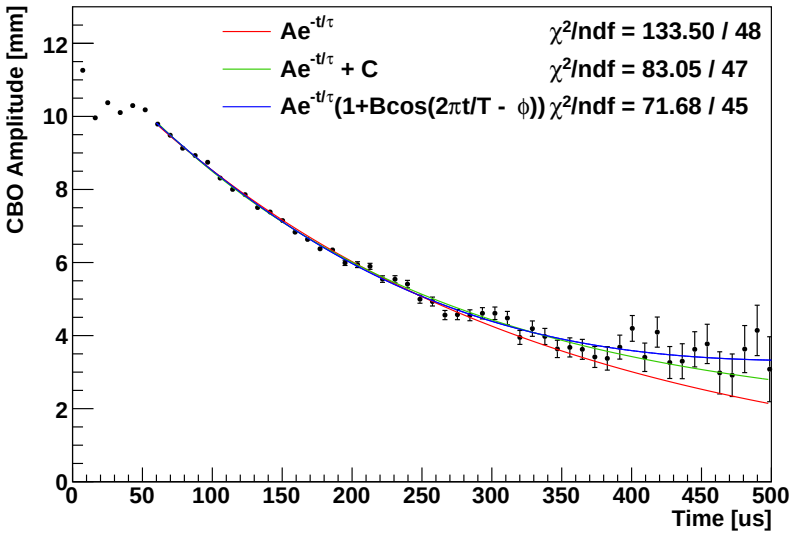

Figure 4.9: Plotted is the CBO amplitude as a function of time from the tracker analysis. Three separate fit functions were used with varying degrees of success to characterize the envelope shape of the CBO (excepting the cosine modulation part). A Gaussian fit was tried with no success. The amplitude isn't fully understood at early times. The period $T/2\pi$ has a value of 114.5 μs. Plot producd by James Mott.

-21.1 ppb and -9.6 ppb respectively, though neither showed any improvement in the fit. (In the latter the period of the oscillatory term was fixed and the other parameters were allowed to float.) I take the latter value of 21.1 ppb as the systematic error on R due to the shape.

4.4.3 CBO Lifetime

Because the CBO lifetime has been fixed in the fit, there is a systematic error on R. Scanning over various values of the fixed CBO lifetime allows this error to be calculated. The resulting curve of R vs the CBO lifetime turns out not to be linear, as shown in Figure 4.10. Taking the uncertainty on the CBO lifetime as the error produced by the T Method fit, approximately 16 μs, and looking at the change in R for CBO lifetime values of 180 ± 16 μs, the systematic error on R is taken as the larger of the two at 12.1 ppb.

4.5 Sensitivity of ω_a to VW function

As described in Section 2.8, the vertical waist does not need to be included in the ratio fit. In order to calculate a systematic error from excluding the VW, I added the VW to the fit as described in that section, with an exponentially decaying cosine term. Since the fit is unstable in regards to the amplitude and lifetime parameters, I fixed them to values

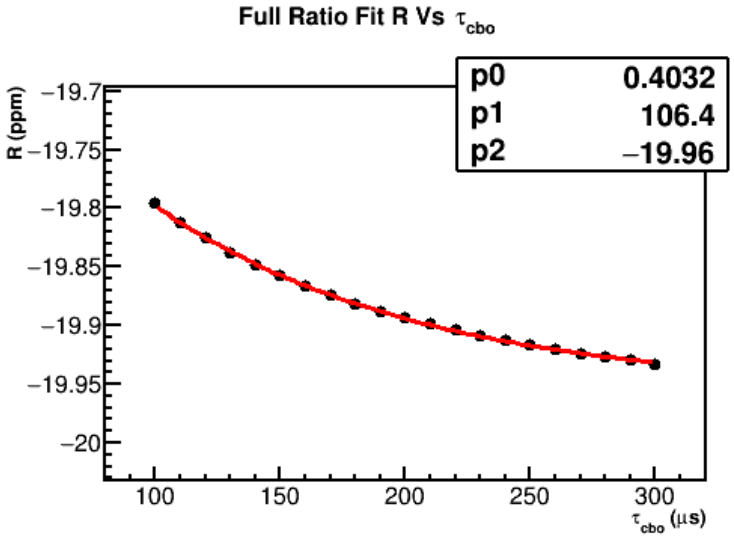

Figure 4.10: Plotted is the fitted R value as a function of the CBO lifetime, which has been fixed in the full ratio fit. The error bars have been removed from the plot in order to show the shape of the curve better. The points have been fitted to an exponential function which lines up nicely, $p_0 e^{-t/p_1} + p_2$.

determined from a T Method fit of the same data. The results can be seen in Figure 4.11. The final fitted R value differs from the non-VW fitted function by less than 1 ppb. This is unsurprising since I'm trying to fit an effect which does not exist in the ratio.

4.6 Sensitivity of ω_a to various effects

More effects to be studied - results vs bunch number, higher order beam/CBO effects, etc.

4.6.1 $g-2$ Period Guess

To perform the ratio method, the $g-2$ period needs to be known a priori to high precision. By scanning over various $g-2$ period guesses the dependence of R on T_a can be determined, as shown in Figure 4.12. The systematic error can then be calculated as

$$\delta R_{period} = \delta\alpha_{period} \times \frac{dR}{d\alpha_{period}} \tag{4.9}$$

where $\delta\alpha_{period}$ is the uncertainty on T_a. Very conservatively taking the uncertainty as 10 ppm, the systematic error on R is calcualted as $10\,\text{ppm} \times 1.62 \times 10^{-4}\,\text{ppm/ppm} = 1.62\,\text{ppb}$, which is completely negligible.

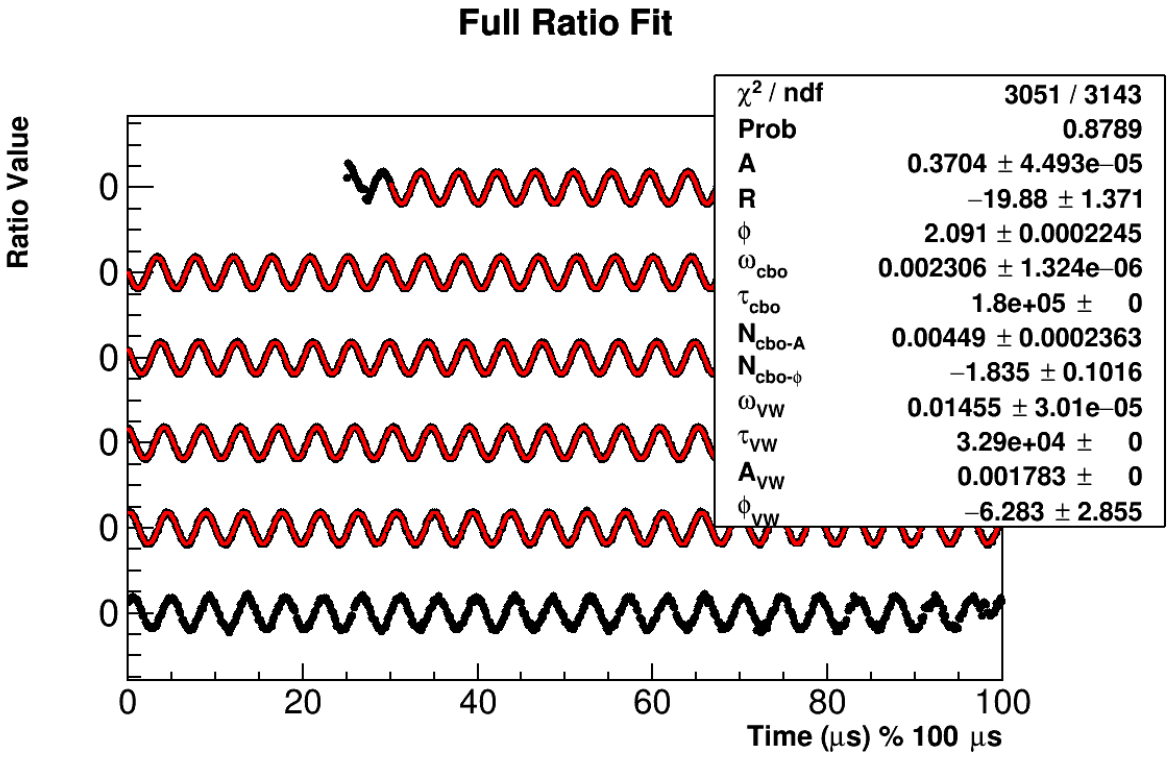

Figure 4.11: Fit results with the VW term included. The lifetime and amplitude of the effect have been fixed, while the frequency and phase are allowed to float. As can be seen there is a large error on the phase. The x axis is in units of μs modulo 100 μs, with successive portions of the data points and fit shifted downwards on the plot. The parameter values in the stats box for the CBO frequency and lifetime are in units of ns. R is blinded locally. The fit ranges from 30 μs to 500 μs.

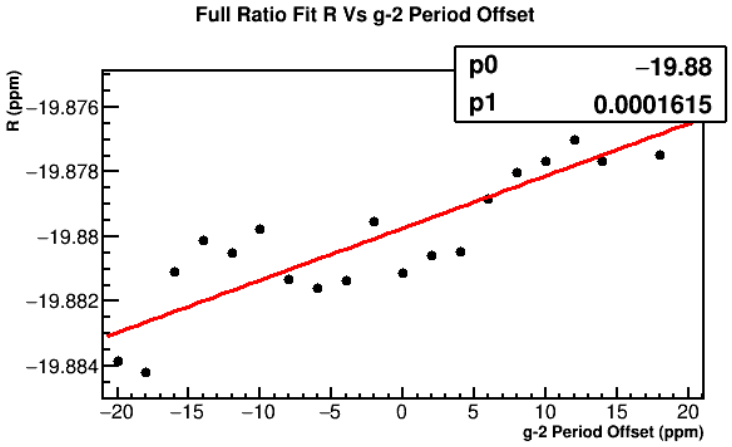

Figure 4.12: Fitted R value as a function of the ppm level offset from the guess used for the $g-2$ period, 2.2. Error bars have been removed from this plot, otherwise it appears as a flat line. The slope is .16 ppb per ppm offset in T_a.

4.6.2 Lifetime used in weighting

Similarly to the $g-2$ period guesses used when constructing the time spectra for the ratio method, the lifetime of the muon is used when splitting the counts into the various histograms with different weights, as seen in Equation A.17. To check for a systematic effect on R from getting this lifetime wrong, I scanned over a range of such lifetimes around the default value used, 64.4 μs. As shown in Figure 4.13, the slope is 2.632 ppb per μs. Since the uncertainty on the lifetime is much less than a microsecond, this systematic error is completely neglible.

4.6.3 Bin Width

The systematic uncertainty from the bin width, chosen to eliminate the fast rotation signal, was calculated by performing the histogramming and fitting stages with varying values of bin widths. The systematic uncertainty is taken as the RMS spread of the fitted R values. As shown in Figure 4.14 it is 44.5 ppb.

4.6.4 Randomization

In the histogramming phase of my analysis, random seeds are used in two places. One for the randomization of counts into the 4 separate datasets that go into the ratio, and one for the time randomization to reduce the fast rotation. It's necessary to make sure that results are consistent among random seeds, and that the final answer wasn't a particularly fortuitous or disastrous choice. In order to test this I performed fits with 20 different random seeds, the χ^2/NDF and fitted R values of which are plotted in Figure 4.15. Results are consistent and very much within error of each other. I also performed fit start scans for a couple of the

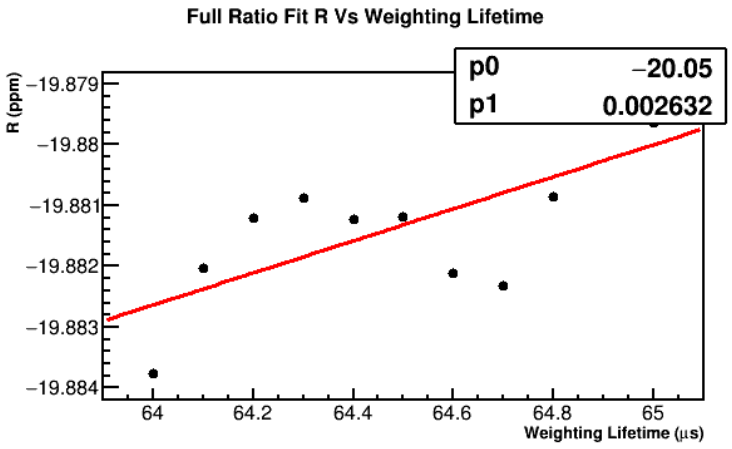

Figure 4.13: Fitted R value as a function of the lifetime used in the weighting of counts into histograms. Error bars have been removed from this plot, otherwise it appears as a flat line. The slope is 2.632 ppb per μs.

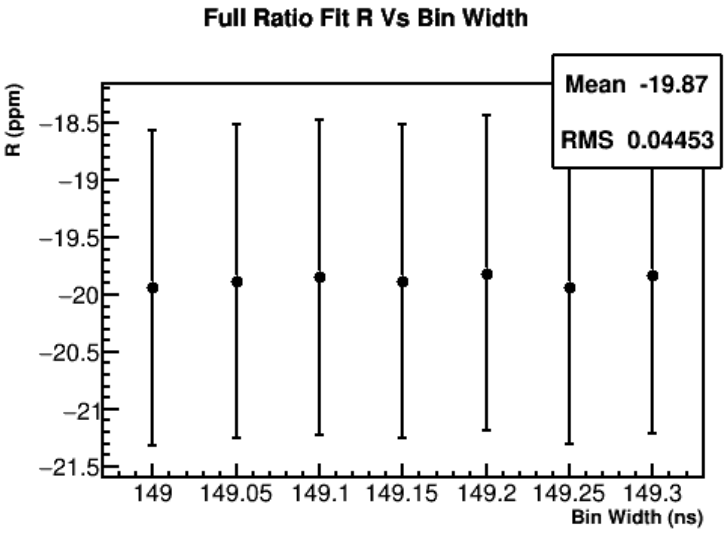

Figure 4.14: Plotted are fitted R values for varying bin widths ranging from 149.00 ns to 149.30 ns in steps of 5 ns.

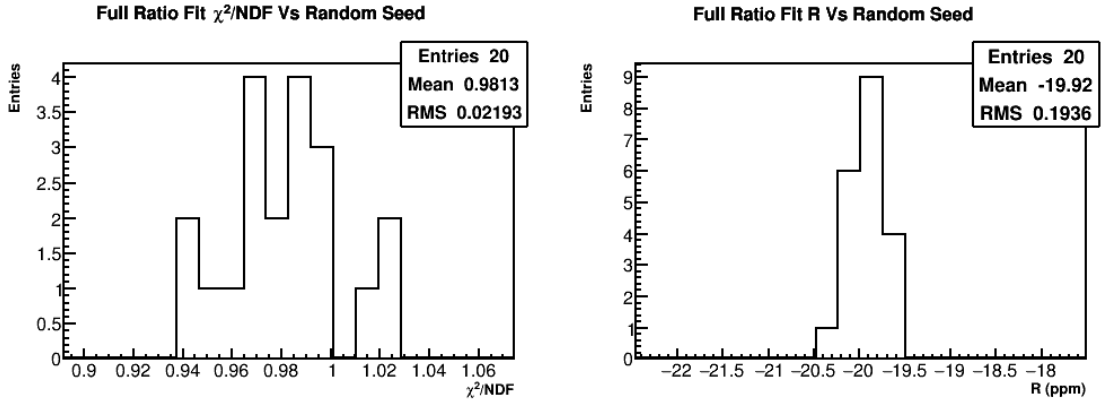

(a) χ^2/NDF values for 20 random seeds.

(b) R values for 20 random seeds.

Figure 4.15: Plotted is the χ^2/NDF and fitted R value for 20 random seeds.

random seeds as an extra check to make sure the fitting was behaving consistently as shown in Figures 4.16 and 4.17.

I'm not so sure there should be a systematic error on R due to the randomization. Such an error should be contained within the statistical error of the final answer I believe. However I calculate one here for posterity in the manner that was done for E821,

$$\delta R_{rand} = \sigma(R)/\sqrt{N-1}, \tag{4.10}$$

where $\sigma(R)$ is the RMS spread in R and N is the number of random seeds fitted, in this case 20. Therefore with an RMS on R of 193.6 ppb, the systematic error on R due to the randomization is (potentially) 44.4 ppb. (The fact that simply increasing the number of seeds allows for this systematic error to reduce to zero as shown in Equation 4.10 gives greater weight to the argument that this really shouldn't be a systematic error at all, and is instead a purely statistical effect already taken care of in the fit.)

4.6.5 Bunch Number

I will examine R for the 8 separate bunches, once the new dataset is available.

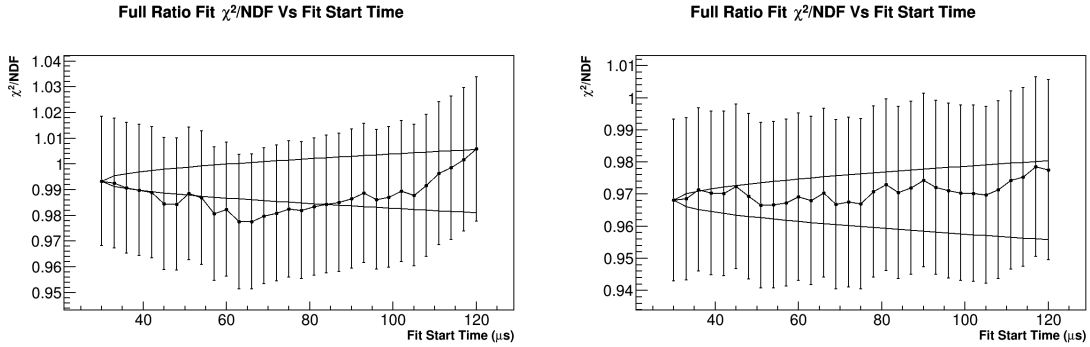

(a) Seed 1

(b) Seed 2

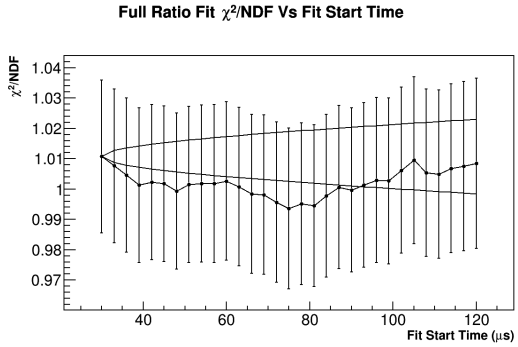

(c) Seed 3

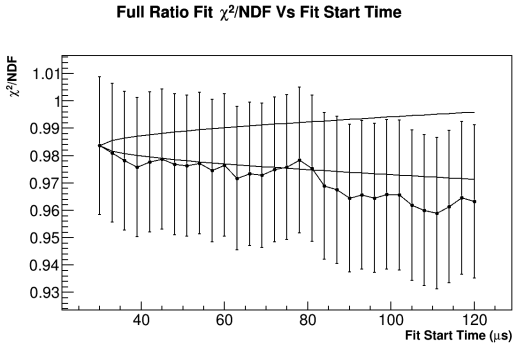

(d) Seed 4

Figure 4.16: Fit start time scans for the χ^2 for four random seeds of the randomization of the same dataset. Compare to Figure **??**. The general behaviour of the fits vs fit start time is consistent and relatively the same, but as is seen the scans can rise and fall at different points due to the choice of randomization.

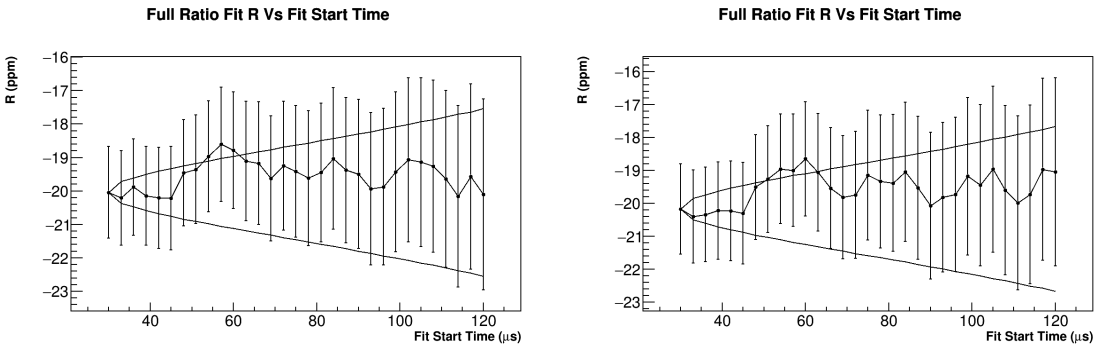

(a) Seed 1

(b) Seed 2

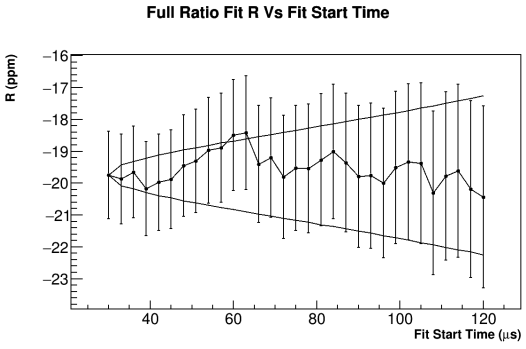

(c) Seed 3

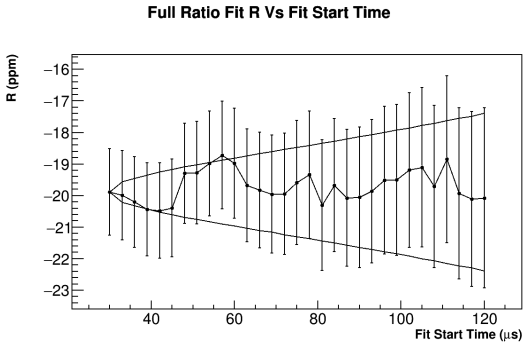

(d) Seed 4

Figure 4.17: Fit start time scans for the fitted R parameter for four random seeds of the randomization of the same dataset. The general behaviour of the fits vs fit start time is consistent.

4.7 Final Systematic Uncertainty Table

Summary of Systematic Errors	
Systematic Error	60 H
Gain(incomplete)	24.8
Pileup	37.8
Lost Muons(incomplete)	36.1
CBO	38.6
VW	< 1
Bin Width	44.5
Randomization	44.4
Bunch Number	
Other	
Total	

Table 4.1: Systematic error table for the 60H dataset. All units are in ppb.

Chapter 5

Conclusion and Final Results

- $R = -19.88 \pm 1.373\,\text{ppm} \pm syst.$ (blinding with common string)
- $\chi^2/NDF = 3052/3145$

Appendix A

Ratio Method Derivation and Fit Function

Consider the 5 parameter function:

$$N_5(t) = N_0 e^{-t/\tau}(1 + A\cos(\omega_a t + \phi)), \tag{A.1}$$

which describes some ideal dataset in histogram format. Here ϕ will be set to zero for simplicity. Now define the variables $u_+(t)$, $u_-(t)$, $v_1(t)$, and $v_2(t)$ as

$$\begin{aligned} u_+(t) &= \frac{1}{4}N_5(t + T/2) \\ u_-(t) &= \frac{1}{4}N_5(t - T/2) \\ v_1(t) &= \frac{1}{4}N_5(t) \\ v_2(t) &= \frac{1}{4}N_5(t), \end{aligned} \tag{A.2}$$

where the 1/4 out front reflects randomly splitting the whole dataset into 4 equally weighted sub-datasets, and T is the g-2 period known to high precision, $\mathcal{O}(10^{-6})$. This corresponds to a weighting of 1:1:1:1 between the datasets. To be explicit here regarding the signs, the counts that are filled into the histogram described by u_+ have their times shifted as $t \to t - T/2$, which is what the function $N_5(t + T/2)$ describes, and vice versa for u_-. To form the ratio define the variables:

$$\begin{aligned} U(t) &= u_+(t) + u_-(t) \\ V(t) &= v_1(t) + v_2(t) \\ R(t) &= \frac{V(t) - U(t)}{V(t) + U(t)}. \end{aligned} \tag{A.3}$$

Plugging in and dividing the common terms $(N_0 e^{-t/\tau}/4)$,

$$R(t) = \frac{2(1 + A\cos(\omega_a t)) - e^{-T/2\tau}(1 + A\cos(\omega_a t + \omega_a T/2)) - e^{T/2\tau}(1 + A\cos(\omega_a t - \omega_a T/2))}{2(1 + A\cos(\omega_a t)) + e^{-T/2\tau}(1 + A\cos(\omega_a t + \omega_a T/2)) + e^{T/2\tau}(1 + A\cos(\omega_a t + \omega_a T/2))}. \tag{A.4}$$

Now set $\omega_a T/2 = \delta$, and note that T is really

$$\begin{aligned} T = T_{guess} &= \frac{2\pi}{\omega_a} + \Delta T, \\ \Delta T &= T_{guess} - T_{true}. \end{aligned} \tag{A.5}$$

Being explicit,

$$\delta = \frac{\omega_a}{2} T_{guess} = \frac{\omega_a}{2}(\frac{2\pi}{\omega_a} + \Delta T) = \pi + \pi \frac{\Delta T}{T_{true}} = \pi + \pi(\delta T), \tag{A.6}$$

and δ can be redefined as

$$\delta = \pi(\delta T), \tag{A.7}$$

by flipping the sign of any cosine terms that contain δ.

Then, using the trig identity

$$\cos(a \pm b) = \cos(a)\cos(b) \mp \sin(a)\sin(b) \tag{A.8}$$

so that

$$\begin{aligned} \cos(\omega_a t \pm \delta) &= \cos(\omega_a t)\cos\delta \mp \sin(\omega_a t)\sin\delta \\ &\approx \cos(\omega_a t)(1-\delta^2) \mp \sin(\omega_a t)\delta \\ &\approx \cos(\omega_a t), \end{aligned} \tag{A.9}$$

since $\delta \sim O(10^{-5})$, the ratio becomes

$$R(t) \approx \frac{2(1 + A\cos(\omega_a t)) - (1 - A\cos(\omega_a t))(e^{-T/2\tau} + e^{T/2\tau})}{2(1 + A\cos(\omega_a t)) + (1 - A\cos(\omega_a t))(e^{-T/2\tau} + e^{T/2\tau})}. \tag{A.10}$$

Expanding

$$e^{\pm T/2\tau} = 1 \pm \frac{T}{2\tau} + \frac{1}{2}\Big(\frac{T}{2\tau}\Big)^2 \pm \ldots, \tag{A.11}$$

repacing and simplifying,

$$R(t) \approx \frac{A\cos(\omega_a t) - C(1 - A\cos(\omega_a t))}{1 + C(1 - A\cos(\omega_a t))}, \tag{A.12}$$

where

$$C = \frac{1}{16}\Big(\frac{T}{\tau}\Big)^2 \approx 2.87 * 10^{-4}. \tag{A.13}$$

Using the expansion

$$f(x) = \frac{1}{1+x} = 1 - x + x^2 - \ldots, \quad |x| < 1, \tag{A.14}$$

and since C is small, the denominator can be manipulated such that

$$\begin{aligned} R(t) &\approx (A\cos(\omega_a t)) - C(1 - A\cos(\omega_a t)))(1 - C(1 - A\cos(\omega_a t))) \\ &\approx A\cos(\omega_a t) - C + CA^2\cos^2(\omega_a t), \end{aligned} \tag{A.15}$$

after dropping terms of $\mathcal{O}(C^2)$ and higher. In practice the last term is ommitted since it has a minimal effect on the fitted value of ω_a [**cite**], and one arrives at

$$R(t) \approx A\cos(\omega_a t) - C, \tag{A.16}$$

the conventional 3 parameter ratio function.

In order to avoid approximations one can instead weight the counts in the histograms as

$$u_+(t) : u_-(t) : v_1(t) : v_2(t) = e^{T/2\tau} : e^{-T/2\tau} : 1 : 1, \tag{A.17}$$

so that

$$\begin{aligned} u_+(t) &= \frac{e^{T/2\tau}}{2 + e^{T/2\tau} + e^{-T/2\tau}} N_5(t + T/2) \\ u_-(t) &= \frac{e^{-T/2\tau}}{2 + e^{T/2\tau} + e^{-T/2\tau}} N_5(t - T/2) \\ v_1(t) &= \frac{1}{2 + e^{T/2\tau} + e^{-T/2\tau}} N_5(t) \\ v_2(t) &= \frac{1}{2 + e^{T/2\tau} + e^{-T/2\tau}} N_5(t). \end{aligned} \tag{A.18}$$

(These factors out front aren't so far off from 1/4 since $e^{\pm T/2\tau} \approx e^{\pm 4.35/2*64.4} \approx 1.034, .967$.) Then instead $R(t)$ becomes

$$R(t) = \frac{2(1 + A\cos(\omega_a t)) - (1 - A\cos(\omega_a t + \delta)) - (1 - A\cos(\omega_a t - \delta))}{2(1 + A\cos(\omega_a t)) + (1 - A\cos(\omega_a t + \delta)) + (1 - A\cos(\omega_a t + \delta))}, \tag{A.19}$$

where the $e^{\pm T/2\tau}$ terms out front now cancel. Using Equation A.9 again and this time avoiding approximations in δ,

$$R(t) = \frac{2A\cos(\omega_a t)(1 + \cos\delta)}{4 + 2A\cos(\omega_a t)(1 - \cos\delta)}, \tag{A.20}$$

after simplifying. In the limit that

$$\delta = \pi(\delta T) \to 0 \tag{A.21}$$

since δT is small,

$$R(t) \approx A\cos(\omega_a t), \tag{A.22}$$

with the only approximation being made at $\mathcal{O}(\delta^2) \sim \mathcal{O}(10^{-10})$.

Finally, while the 3 parameter ratio function suffices for fits to data containing slow modulations, it does not suffice for faster oscillation features. In that case it is more useful to fit with the non-approximated or simplified version of the ratio,

$$\begin{aligned} R(t) &= \frac{v_1(t) + v_2(t) - u_+(t) - u_-(t)}{v_1(t) + v_2(t) + u_+(t) + u_-(t)}, \\ &= \frac{2f(t) - f_+(t) - f_-(t)}{2f(t) + f_+(t) + f_-(t)}, \end{aligned} \tag{A.23}$$

where

$$\begin{aligned} f(t) &= C(t)(1 + A\cos(\omega_a t + \phi)) \\ f_\pm(t) &= f(t \pm T_a/2), \end{aligned} \tag{A.24}$$

and $C(t)$ can encode any other effects in the data that need to be fitted for, such as the CBO,

$$C(t) = 1 + A_{cbo} e^{-t/\tau_{cbo}} \cos(\omega_{cbo} t + \phi_{cbo}). \tag{A.25}$$

Additionally, any other fit parameters such as A or ϕ can be made a fuction of t. Using the non-approximated form for the final fit function gives greater confidence in the fit results for the high precision ω_a extraction necessary for the experimental measurement.

Appendix B

Ratio Method Errors